NOTICE

The quality of this microform is heavily dependent upon the quality of the original thesis submitted for microfilming. Every effort has been made to ensure the highest quality of reproduction possible.

If pages are missing, contact the university which granted the degree.

Some pages may have indistinct print especially if the original pages were typed with a poor typewriter ribbon or if the university sent us an inferior photocopy.

Reproduction in full or in part of this microform is governed by the Canadian Copyright Act, R.S.C. 1970, c. C-30, and subsequent amendments.

AVIS

La qualité de cette microforme dépend grandement de la qualité de la thèse soumise au microfilmage. Nous avons tout fait pour assurer une qualité supérieure de reproduction.

S'il manque des pages, veuillez communiquer avec l'université qui a conféré le grade.

La qualité d'impression de certaines pages peut laisser à désirer, surtout si les pages originales ont été dactylographiées à l'aide d'un ruban usé ou si l'université nous a fait parvenir une photocopie de qualité inférieure.

La reproduction, même partielle, de cette microforme est soumise à la Loi canadienne sur le droit d'auteur, SRC 1970, c. C-30, et ses amendements subséquents.

ISBN 0-315-56047-9

Canada

Synthesis and Spectroscopic Studies of Cr^{3+} doped glasses and transparent glass ceramics of the Magnesium Alumino Silicate system $MgO.Al_2O_3.2.5SiO_2$.

Nick Raspa

A Thesis
in
The Department
of
Chemistry

Presented in Partial Fulfillment of the Requirements for the
Degree of Master of Science
at Concordia University
Montréal, Quebec, Canada

February 1990

ABSTRACT

Synthesis and Spectroscopic Studies of Cr^{3+} doped glasses and transparent glass ceramics of the Magnesium Alumino Silicate system $MgO.Al_2O_3.2.5SiO_2$.

Nick Raspa

This thesis reports the luminescence of Cr^{3+} in the magnesium alumino silicate glass systems ($XMgO.Al_2O_3$-$.2.5SiO_2$, X = 0.5 - 2.0) using laser spectroscopy. Glasses and glass ceramic of high optical quality can be easily synthesized in the $XMgO.Al_2O_3.2.5SiO_2$ system simply by varying X (0.5-2.0) without recourse to thermal treatment. Evidence that Cr^{3+} resides in both the crystalline phase and glass phase of the glass ceramic is presented. Furthermore the crystalline phases are identified as Al_2O_3, and $MgAl_2O_4$ and the glass phases as mullite ($3Al_2O_3.2SiO_2$) and cordierite ($MgO.Al_2O_3.2.5SiO_2$).

In the cordierite glass emission is observed from two levels (^2E_g and $^4T_{2g}$). The room temperature and low temperature Cr^{3+} fluorescence in cordierite glass is dominated by strong $^4T_{2g}$ emission in which the $^4T_{2g}$ fluorescence extends from 730 to 870 nm. Within the sample, there are centers that can be characterized as low, intermediate and high field.

We were able to determine that the system presents an intermediate crystal field for Cr^{3+} ions (Dq/B = 2.00). The complex spectroscopic features of Cr^{3+} in cordierite glass are mainly due to the large inherent inhomogeneity of the material. As a result the energy separation and the order of the two emitting states ($^4T_{2g}$ and ^2E_g) vary from site to site leading to a large inhomogeneous broadening of absorption and emission spectra and complex decays of luminescence. The $^4T_{2g}$, $^4T_{1g} \longleftarrow {}^4A_{2g}$ transitions in cordierite glass showed the maximum oscillator strengths of 1.81×10^{-4} and 3.37×10^{-4} respectively. This can be explained on the basis of the large inhomogeneity of the material.

Since Cr^{3+} is sensitive to the environment, structural changes occuring during crystallization become evident in the spectra as the MgO concentration is changed. We observed that crystallization is accompanied by a relative increase in emission from the $^2E_g \longrightarrow {}^4A_{2g}$ transition as well as narrowing and splitting of the corresponding band. This we related to the higher crystal field and the narrow distribution of Cr^{3+} sites generally observed in crystals. The splitting of the ^2E_g was found to be 30 cm^{-1} (ruby, 29 cm^{-1}).

Cordierite glass doped with 0.17 % Cr_2O_3 was subjected to a heat treatment in order to induce complete ceramtization.

The emission spectra and X-ray diffraction pattern of the ceramic revealed that the crystalline phase is the magnesium spinel $MgAl_2O_4$. The emission spectra is characterized by N_3 lines centered at 686 and 688 nm that can be interpreted to arise from Cr^{3+} ions in different environments due to cation inversion effects. Another line was obseved at 710 nm and was attributed to chromium pair interaction due to concentration effects.

ACKNOWLEDGEMENT

I wish to thank my research supervisor, Dr. J.A. Capobianco, for his keen interest, patience, valuable guidance and direction throughout the course of this work and in the preparation of this thesis.

I would like to thank the members of my research committee, Drs. P.H. Bird and C.H. Lanford for their helpful suggestions and Dr. M. Lawrence for his critical comments on the thesis.

I am particularly indebted to Dr. A. Monteil for the low temperature absorption spectra and the stimulating discussions on some aspects of this research. I would also like to thank Dr. G. Dénès for performing the X-ray diffraction on the cordierite ceramic.

I especially thank my colleague and dear friend Pierre Paul Proulx for his encouragement and companionship during the many long hours of work.

I also thank Guy Cormier, Allan Bruce, and Bruno Adrinanosolo for their help and camaraderie. The assistance of Marco Raspa for producing some of the figures was particularly helpful.

Dedicated to my parents

and Annie

TABLE OF CONTENTS

CHAPTER 3

CHAPTER 4

FIGURE CAPTIONS

TABLE CAPTIONS

CHAPTER 1

1. INTRODUCTION

Although glass is a solid, it is more typically recognized as a solid solution or a "frozen liquid" that possesses a continuous random network lacking both symmetry and periodicity. For spectroscopists and material scientists, the relative allure of using glass as a possible laser relative to a crystal is that a glass can be "engineered". Glasses have always held a fascination because of the variety of their compositions, which gives a certain amount of control over their properties [1]. Glasses possess excellent optical quality, are optically isotropic, durable, and can be doped with transition and rare earth metals to high concentrations. Furthermore, glass can be molded to any shape and size.

1.1 STRUCTURAL MODEL FOR GLASS

According to the traditional views held by Zachiarisen [2] which are still valid today, the constituent cations in a glass are divided into network formers and network modifiers. The basic structural units which make up the glass consist of compounds that have a definite geometry and are connected at corners to form a random three dimensional network.

Network formers exhibit either 3 or 4 coordination to form triangles or tetrahedra which are cross linked by corner sharing into closed network structures [3]. Intermediate or conditional glass formers require the presence of one or more additional compounds to form the glass. Other compounds added to the glass modify the network, thus anions which formally bridged two network forming cations may become nonbridging. Network modifiers such as alkali, alkaline earth, and higher valence state ions occupy interstitial sites, usually thought of as 6 coordinating.

Sun [4], categorized oxide compounds as glass formers, intermediates, or modifiers on the basis of their calculated bond strength shown in Table 1.1.1. Glass formers generally have bond energies above 100 kilocalories; intermediates have bond energies of 60 to 73 kilocalories ; and modifiers have bond energies below 60 kilocalories.

1.2 ACTIVATOR IONS IN GLASS

The colors imparted to glasses that serve as host to transition metal ions have attracted attention since the early history of glass making [5]. In the period 1950 to the 1960's, crystal field theory was applied to gain insight into the relation of color to structure. Bates [6] reviews some of the early efforts and Wong and Angell [7] summarize the literature up to 1976.

TABLE 1.1.1

CALCULATED BOND STRENGTH OF OXIDE COMPONENTS

METAL	COORDINATION NUMBER	SINGLE BOND STRENGTH (KILOCALORIES)
	GLASS FORMERS	
B	3	119
Si	4	106
Ge	4	108
Al	3	101
P	5	111
V	5	112
	INTERMEDIATES	
Ti	6	73
Al	6	57
Th	8	64
Be	4	63
Zr	8	61
	MODIFIERS	
Mg	6	37
Li	4	36
Ba	8	33
Ca	8	32
Na	6	20

The behavior of the activator ion in the host material can be explained by means of crystal field theory. The metal ion is considered to be the center of a coordination sphere (polyhedron) formed by ligands. In this theory, the ligands are taken as point charges which create an electrostatic field around the central metal ion. Hence, this model simplifies the calculation of the crystal field parameter Dq, and the Racah parameters relative to ligand field theory.

1.3 TRIVALENT CHROMIUM AS THE ACTIVATOR ION

Over the past years there has been a surge of interset in Cr^{3+}, largely due to its demonstrated ability to lase in various hosts. There are numerous advantages to the Cr^{3+} ion, which include; (i) the stability of the trivalent state against both oxidation and reduction, (ii) the presence of three broad bands and allowing efficient flashlamp pumping, (iii) the resistance of the $^4T_{2g}$ state to nonradiative decay and (iv) the tendency of Cr^{3+} to preferentially occupy octahedral sites in the presence of other types of host sites. To date Cr^{3+} has been reported to lase in 15 materials; $BeAl_2O_4$ [8, 9, 10], $Be_3Al_2(SiO_3)_6$, [11], $Gd_3Sc_2Al_3O_{12}$ [12, 13], $Gd_3Ga_5O_{12}$ [14], $Gd_3Sc_2Al_3O_{12}$ [14], $La_3Lu_2GaO_{12}$ [14], $Y_3Ga_5O_{12}$ [13], $Y_3Sc_2Ga_3O_{12}$ [13], $Na_3Ga_2Li_3F_{12}$ [15], $KZnF_3$ [16], $SiAlF_5$ [17, 18] $ZnWO_4$ [19], $Al_2(WO_4)_3$ [20], $ScBO_3$ [21] and $La_3Ga_2SiO_{14}$ [22].

1.4 STATEMENT OF THE PROBLEM

Luminescence of Cr^{3+} in glasses of the alumino-silicate composition have been studied extensively by Lempecki [23]. The main emphasis was to understand the spectroscopic properties of chromium in this host material (Alumino silicate) for suitability as a laser material. They studied mullite ($2Al_2O_3.SiO_2$), gahnite ($ZnAl_2O_4$) and β-quartz (SiO_2) since these materials possess high tensile strength and very low thermal coefficient of expansion. These properties are a prerequisite for a laser host material.

The principle objective of this work was to systematically study the spectroscopic behaviour of Cr^{3+} in cordierite glass, glass ceramic and ceramic. The mineral cordierite is a complex material whose chemical formula is $Mg_2Al_4Si_5O_{18}$ and capable of accepting a wide variety of cationic impurities substitutionally at the aluminum site. Among various activator ions, Cr^{3+} is especially interesting. The ion is not only a structural probe, but also a "nucleating" agent that induces growth of microcrystallites within the vitreous phase. Spectroscopically, one can also determine, using Cr^{3+} as the structural probe, the microcrystalline phase as the structure evolves from the glassy phase to the crystalline phase via the glass ceramic. The nature of the sites occupied by Cr^{3+} can also be determined.

Optical spectroscopy provides the techniques (absorption, emission, time resolved, lifetime measurements) necessary to calculate the crystal field and Racah parameters so pertinent information can be gained about the system. The optical properties must be fully characterized in cordierite glass before it can be investigated as a potential host matrix for laser technology. At this point, cordierite is promising as a potential laser host material for a number of reasons:

1. Its relative ease of fabrication.

2. Broad absorption bands which maximize coupling to broadband sources, such as flashlamps. Thus, it is capable of storing a greater density of energy.

3. Strong $^4T_{2g}$ fluorescence.

4. Chromium III can satisfy its coordination requirement by substituting as a network former or as a network modifier.

5. High mechanical strength.

2.THEORETICAL

2.1 THE GLASSY STATE

Glass might be described as a transparent substance having the properties of hardness, rigidity and brittleness. With the exception of transparency, the properties usually thought of as characterizing glass are those normally associated with solids. However, glass possesses a number of properties which are characteristic of the liquid state and the classification of glass as a liquid of very high viscosity rather than as a solid would be in accordance with modern views [24].

A definition of what constitutes a glass according to the National Research Council Ad Hoc Committee on Infrared transmitting materials is [25];

A glass is an X-ray amorphous "solid" which exhibits a glass transition T_g, the latter being that phenomenon in which a solid amorphous phase exhibits with changing temperature a more or less sudden change in the derivative thermodynamic properties, such as heat capacity, C_p, and expansion coefficient, from crystal like to liquid like values. The temperature of this is called the glass transition or transformation temperature T_g. Above Tg the amorphous phase has

the thermodynamic properties of the liquid state, hence is referred to as being in the "supercooled liquid", as distinct from the glassy state.

It is useful at this point to consider the relationship between the solid and the liquid state in order to obtain a clearer understanding of glass structure. This implies that a liquid cannot be structureless in the same sense as a gas but that there must be some sort of grouping or arrangement of the molecules in the liquid related to that which occurs in the solid state. The units of structure (atomic or molecular groupings) are the same in the liquid as in the solid but in the liquid these units are not arranged in a regular manner. Hence the liquid possesses short range order whereas the crystalline possesses both short range and long range order leading to complete regularity throughout the solid.

The relationship between the glassy state and the normal solid and liquid states can be understood on the basis of what happens during the ccoling of melts. For substances which crystallize, it is observed that there is a closely defined temperature at which solidification occurs and at this temperature a discontinuos volume change (normally a contraction) occurs.

Furthermore, heat is evolved when solidification takes place. On the other hand, for a substance which can be cooled to the glass state, no discontinous volume change is found and heat is not evolved with the change from the liquid to the solid state. Instead the viscosity of the melt increases progressively as the temperature falls and eventually the viscosity attains values which are about $10^{14.6}$ Poise [26]. This is shown in Figure 2.1.1. The crystallization process is manifested by a *sudden* change in volume at T_m, whereas glass formation is characterized by a "gradual break" in slope. The region over which the change of slope occurs is termed the "glass transition temperature" T_g. Hence, the glassy state is continuous with the liquid state and is distinguished from the normal liquid state by the high magnitude of the viscosity.

2.2 CONDITION FOR GLASS FORMATION

Crystallization of supercooled liquids is controlled by two factors. The first is the nucleation rate i.e. the number of nuclei formed in a unit volume per unit time; the second is the rate of crystal growth, or the speed with which the crystal-liquid moves, i.e. the rate of shift of 'phase ' boundary of the crystalline phase in the liquid. As the crystal grows from a certain number of crystal nuclei these nuclei determine the actual phase transformation.

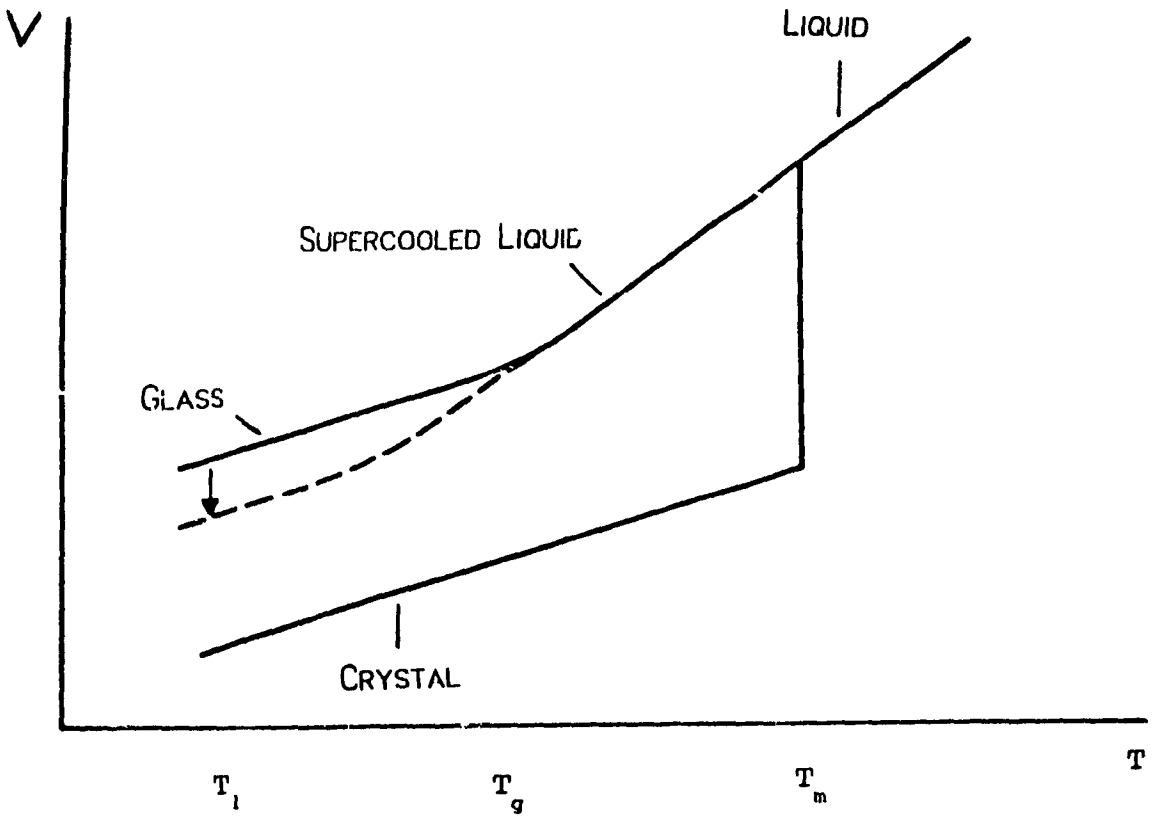

Figure 2.1.1 Schematic illustration of the change in volume with temperature as a supercooled liquid is cooled through the glass transition temperature T_g. The dashed curve illustates the change accompanying the structural relaxation of the glass held at $T < T_g$.

A model based on a quantitative determination of the nucleation rate as a criterion for glass formation was developed by Turnbull [27]. He proposed that no nuclei should be formed as a condition for glass formation: this condition is defined by the relationship

$$n^* = V\int I_0 \, dt \qquad n^* < 1 \qquad (2.2.1)$$

where n^* is the number of nuclei formed in a sample of volume V during cooling time t. He expressed the nucleation rate I_0 in terms of the classical theory of homogeneous nucleation.

An essential prerequisite for "glass formation" from the melt, is that the cooling be sufficiently fast to preclude crystal nucleation and growth, and that the nucleation rate should be less than $10^{-6}cm^{-3}s^{-1}$ [26], not to be observable in practical time scales and liquid volumes. The crystalline phase being thermodynamically more stable, crystal growth will always dominate over the formation of the amorphous phase if allowed to take place.

In 1925, Tammann [28] studied crystallization in supercooled liquids including inorganic glasses which contributed greatly to the knowledge of nucleation and crystallization processes. He showed that below the equilibrium melting temperature there exists a temperature interval, referred to

as the metastable zone, in which nuclei do not form at a detectable rate. In this zone however, crystals can grow if nuclei are provided, i.e. if the melt is "seeded". At temperatures below this region the crystallization process is controlled by two factors: the rate of formation of nuclei and the crystal growth rate. Melts which increase rapidly in viscosity during cooling, such as those which can form glasses, show maxima in nucleation and crystal growth rates because at low temperatures the high viscosity hinders the atomic rearrangements and diffusion processes which are necessary for nucleation and crystal growth. Figure 2.2.1 shows the curves for nucleation rate and crystal growth rate for a viscous melt.

It is evident from Figure 2.2.1 that in order to produce the largest possible number of crystals, nucleation should occur at or near to the temperature at which the maximum nucleation rate occurs. The selection of the optimum nucleation temperature is important in the production of glass ceramics. The metastable zone of supercooling (T_1 - T_2) below the equilibrium temperature occurs because the very tiny crystal nuclei have melting temperatures appreciably below that of the bulk material. It will also be noted that there also exists a temperatuire T_3, below which the homogeneous nucleation rate is zero due to the high viscosity of the melt [29].

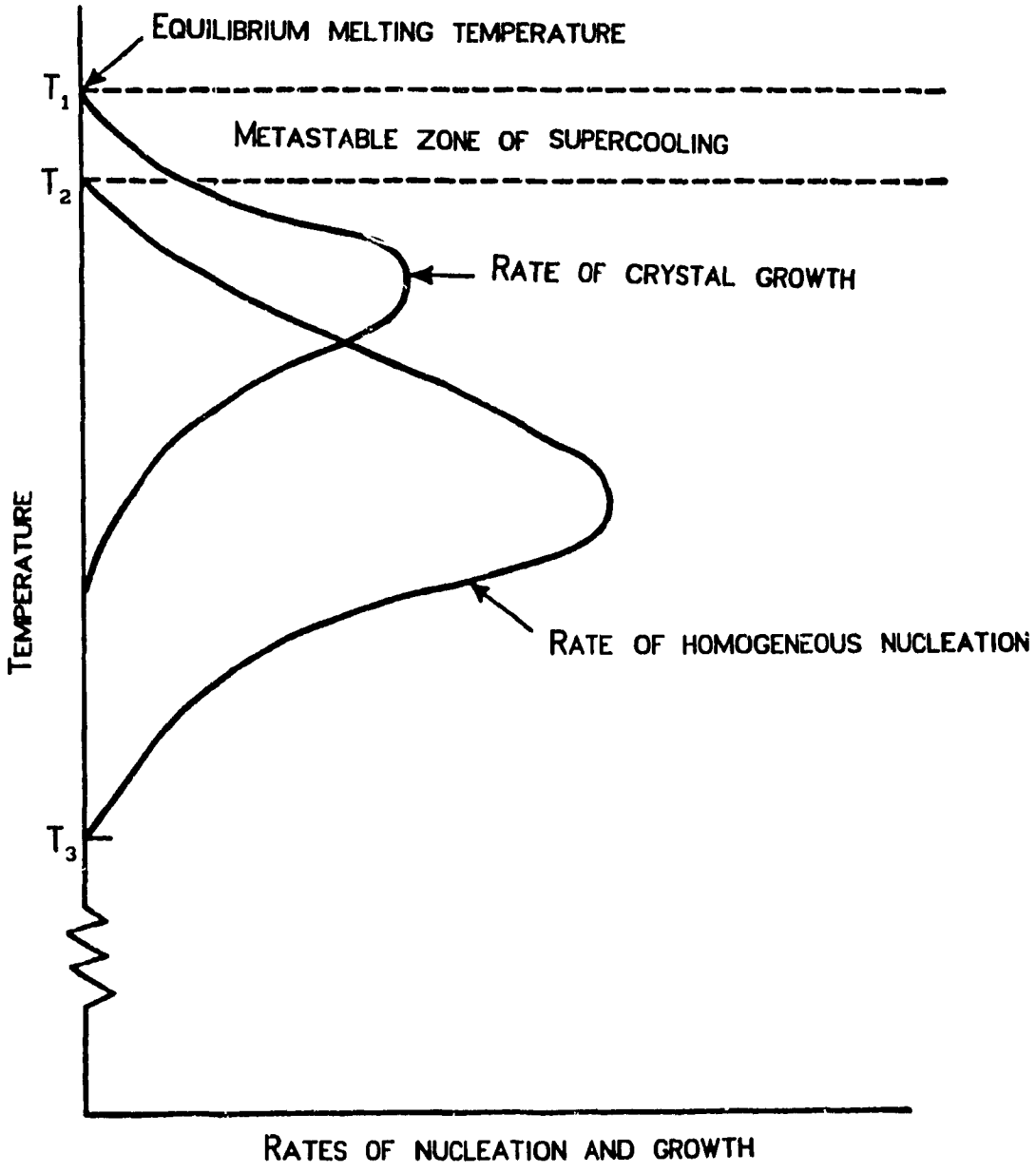

Figure 2.2.1 Effect of temperature on the rates of homogeneous nucleation and crystal growth in a viscous liquid.

2.3 GLASS FORMATION: OXIDE SYSTEMS

The question of "why do certain materials readily form glasses on cooling a melt"? is one of great practical and technological importance. This question may be reformulated as "why do certain chemical compositions of materials have a greater glass forming tendency than others"?. This aspect of the subject is still in the 'alchemy' stage but is nonetheless useful as a guideline for oxide glasses. The first successful attempt to categorize materials into glass-formers and non glass-formers was by Zachariasen (1932) [2]. At the time Zachariasen wrote his paper some 50 years ago, the only known glass-forming materials were oxides, of which only five formed glasses by themselves: SiO_2, GeO_2, B_2O_3, As_2O_3 and P_2O_5. In addition, these five oxides can also form glasses when mixed (up to a limiting percentage) with another oxide or oxides, which are not themselves glass-formers. The rules that Zachariasen formulated were capable of explaining why, for example, SiO_2 is a glass-former and Na_2O is not, but why should $XNa_2O{:}SiO_2$ also be a glass former.

Zachariasen argued that those materials most likely to form glasses readily would have an internal energy only slightly larger in the amorphous state than in the crystalline (a hypothetical amorphous phase possessing an internal energy considerably higher than the crystal would be prone

to rapid devitrification). Since it is reasonable to assume that the interatomic interactions in both amorphous and crystalline phases would be very similar, this implies that the atomic structure of the two phases would be very similar in certain aspects. The structure of the glass network is, however, aperiodic, giving rise to broad diffuse haloes in diffraction patterns instead of sharp spots (or rings) characteristic of the crystalline phase. Therefore Zachariasen assumed that the oxygen polyhedra found in oxide crystals would also occur in glasses, the only difference being the relative orientation of polyhedra which should be variable in glasses, giving rise to a non-periodic structure.

The most important aspect of Zachariasen's approach which transcended the importance of his 'rules' for glass formation was that a non-periodic arrangement of atoms could be attained solely as a result of the incorporation of variation of bond angles and dihedral angles for three dimensions. In this way a continuous random network can be constructed in which the approach of atoms closer than a normal bond length can be avoided, thereby minimizing repulsive energies and hence the total internal energy. The difference in structure for the glassy and crystalline forms of a hypothetical, two dimensional oxide, A_2O_3, is shown schematically in Figure 2.3.1 (a) in which each oxygen is corner

shared by two AO_3 triangles. Contrast this with the case shown in Figure 2.3.1 (b) which is for a hypothetical two dimensional crystalline oxide AO, where each oxygen is corner shared by three AO_3 triangles: structural disorder cannot be introduced as in Figure 2.3.1 (a) simply by bond angle distortion without considerably increasing the internally energy. The amorphous state is metastable since for crystallization to occur a substantial topological rearrangement of the structural units (having a large activation energy) must occur.

Based on these arguments, Zachariasen proposed four rules which an oxide must obey if it is to form a glass:

1. An oxygen atom may be linked to no more than two A atoms.

2. The number of oxygen atoms surrounding an A atom must be small (three or four).

3. The oxygen polyhedra share corners with each other, not edges or faces.

4. At least three corners in each oxygen polyhedron must be shared if the network is to be three dimensional.

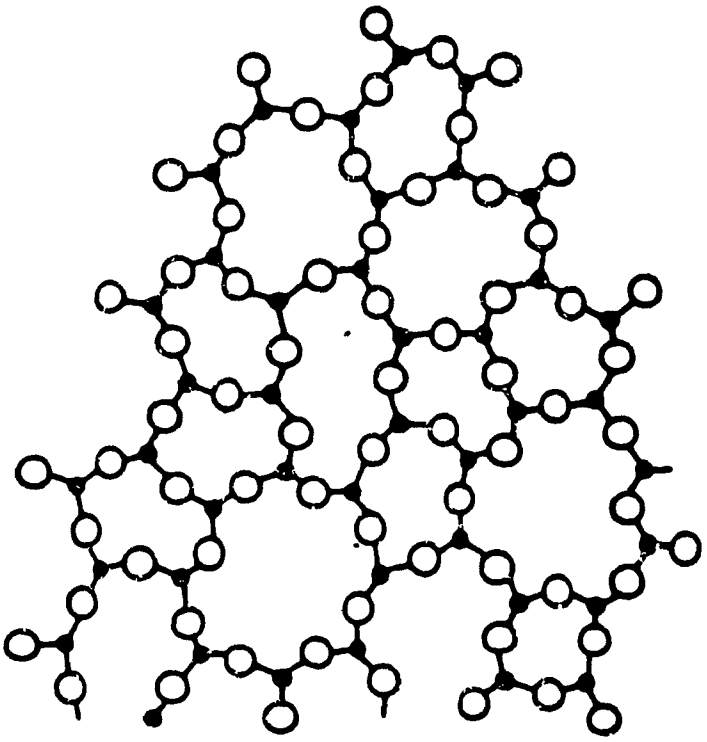

(a)

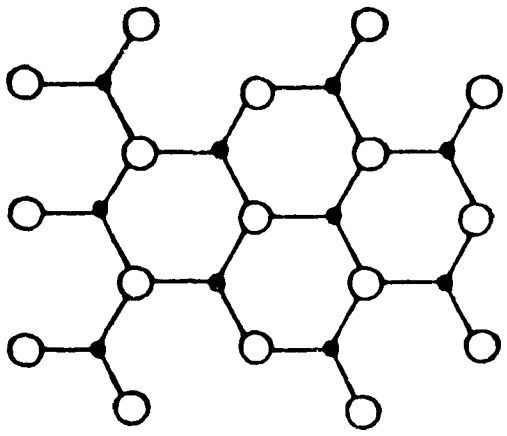

(b)

Figure 2.3.1 Two dimensional representation of amorophous A_2O_3 (a) and crystalline AO (b).

2.4 PHASE SEPARATION

An obvious example of phase separation is the nucleation and growth of crystallites within an amorphous solid. The presence of these inhomogeneities can be detected by small angle scattering (crystallites would produce sharp Bragg peaks if they were of sufficient size) or the more direct technique of microscopy [30]. One cannot underestimate the importance of phase separation. For example, when borosilicate [30] glass is heat treated, it phase separates into a silica rich phase possessing a chemical durability approaching that of vitreous silica. The presence of apparently amorphous structural inhomogeneities from 20 to 200 Å [31] in a number of important commercial glasses has led to the widespread opinion that liquid separation is an essential characteristic of glass structure in general.

The thermodynamic concept of phase separation is useful because of its simplicity. A homogeneous single phase will separate in two (or more) phases of different compositions if the free energy of the system is lower than that of the single homogeneous phase. However, thermodynamics alone does not provide a complete description of why phase separation occurs.

Atomistic consideration of glass structure lead to the hypothesis that reorganization of a glass into two liquids represents the failure of the SiO_4 tetrahedral network to accomadate structural groups of widely different size. As the melt cools to form a glass, the structural positions become more fixed and the SiO_4 groups become less able to join with units of different size and coordination to form a continuous single random network. This is in agreement for the cause of phase separation of the Al_2O_3-SiO_2 system according to Beall and Duke [32]. At high tempeatures, the aluminosilicate liquid is stable as a single phase composed structurally of partially linked SiO_4 and AlO_4 tetrahedra. On cooling the melt polymerizes toward a corner shared tetrahedral arrangement, this increases the internal energy of the system thus producing a siliceous rich phase separated from high alumina regions.

2.5 CONDITION FOR TRANSPARENCY AND FORMATION OF TRANSPARENT GLASS CERAMIC

The most important optical property for transparent glass ceramic is transmission of radiation. The passage of light is affected primarily by the crystal size. Most ceramics are opaque because they are composed of crystallites that act as scattering centers for visible light [32]. The intensity of the scattered light ($I(\theta)$) is written

as:

$$I(\theta)=\left(\frac{1+\cos^2\theta}{r^2}\right)\frac{8\pi^4}{\lambda^4}\alpha^6\left|\frac{M^2-1}{M^2-2}\right|I_o \qquad (2.5.1)$$

where I is the specific intensity, θ the scattering angle, r the distance from the scattering center, I_o the intensity of the incident beam, λ the wavelength of light, α the radius of the particle, and M the ratio of the refractive index of the particle to that of the surrounding medium.

Therefore the criteria for complete transparency in a light transmitting material are (i) $\alpha << \lambda$, where the particles are much smaller than the wavelength of light, or (ii) $M \cong 1$, where the ratio of the refractive indicies of the particles and surrounding medium approach unity. In case (i), the crystallites must be sufficiently small to produce no effective scattering in the visible spectrum. This is the situation in the Al_2O_3-SiO_2 system, where such glass ceramics contain a fine dispersion of crystallites in the siliceous phase [33].

2.6 SPECTROSCOPY OF THE TRANSITION METALS

2.6.1 CRYSTAL FIELD THEORY

In crystal field theory a complex is assumed to be an ionic molecule and the ligands act as point charges providing a constant electric potential.

The one electron Schrödinger equation is;

$$\hat{\mathcal{H}}\,\Psi = E\,\Psi \qquad (2.6.1.1)$$

where the Hamiltonian operator for the hydrogen atom is

$$\frac{-h^2}{8\pi^2 m}\nabla^2 - \frac{e^2}{r} \qquad (2.6.1.2)$$

where m is the mass of an electron, h is Plank's constant, ∇^2 is called the Laplacian operator, and r is the distance of the electron from the nucleus.

The first term expresses the kinetic energy, and the second, the potential energy of the electron. For a many electron system and the case where the central ion becomes complexed the modified Hamiltonian will also include the perturbing potential provided by the field of the ligands and is conveniently written in the form [34].

$$\hat{\mathcal{H}} = \frac{-h^2}{8\pi^2 m}\sum \nabla_i^2 - \sum \frac{Ze}{r_i} + \sum_{i>j}\frac{e^2}{r_{ij}} + \sum \xi_i(r_i) l_i s_i + \sum V_i \qquad (2.6.1.3)$$

The term V_i appears in the Hamiltonian to account for the energy of interaction between the electrons and the crystal field. One considers how V compares in magnitude to the two perturbations in the free atom; the Coulomb repulsion term $\left(\sum_{i>j}\frac{e^2}{r_{ij}}\right)$, and the spin orbit coupling term $\left(\sum \xi_i(r_i) l_i s_i\right)$. Two approaches to the calculation of the

energy levels of d^n systems have developed, arising from two limiting conditions (weak and strong field) described in the following section.

2.6.2 WEAK FIELD AND STRONG FIELD APPROACHES

Calculations on the relative positions of energy levels were started by Orgel [35] in 1952 using the weak field approach . The ligand field is treated as a pertubation term which splits the free ion states but does not cause them to interact with one another. The calculation is carried out by including the interaction between states having the same total spin angular momentum S and Γ, where Γ is a label which indicates the irreducible representation of the octahedral group to which the eigenstate belongs, due to the ligand field. The results of the calculation are expressed as energy matrices, each corresponding to a particular $^{2S+1}\Gamma_n$.

Tanabe and Sugano evaluated the complete strong field calculations for d^n systems in octahedral symmetry. They treated the electrostatic interaction as a pertubation which splits the ligand field configurations but does not cause intermixing of different configurations. A complete calculation is carried out for states having the same S and Γ due to the electrostatic interaction. The results of the calculation are expressed as energy matrices each cor-

responding to a particular $^{2S+1}\Gamma$. The non-diagonal elements of the matrices contain Racah parameters , which represent the interaction between different ligand field states.

2.6.3 TANABE SUGANO DIAGRAMS

Tanabe and Sugano used the strong field approach to calculate the energy level diagrams for the d^n configuration. When the values of E/B are plotted against Dq/B for a specific value of C/B, the result is the Tanabe-Sugano diagram. The essential feature in the Tanabe-Sugano diagrams is that the zero in energy is taken as the lowest lying state arising from the lowest free atom term. Forcing this state to correspond to the abscissa of the diagram, for all values of Dq/B results in raising any point of any state by the amount that was required to keep the lowest lying state on the abscissa. The solution of the energy matrices for a d^3 configuration results in the Tanabe-Sugano diagram given in Figure 2.6.3.1. The diagram is drawn only up to a value of Dq/B = 4. This value of Dq is large enough for the states of the ion to occur in the same sequence as they were assigned in the "strong field case".

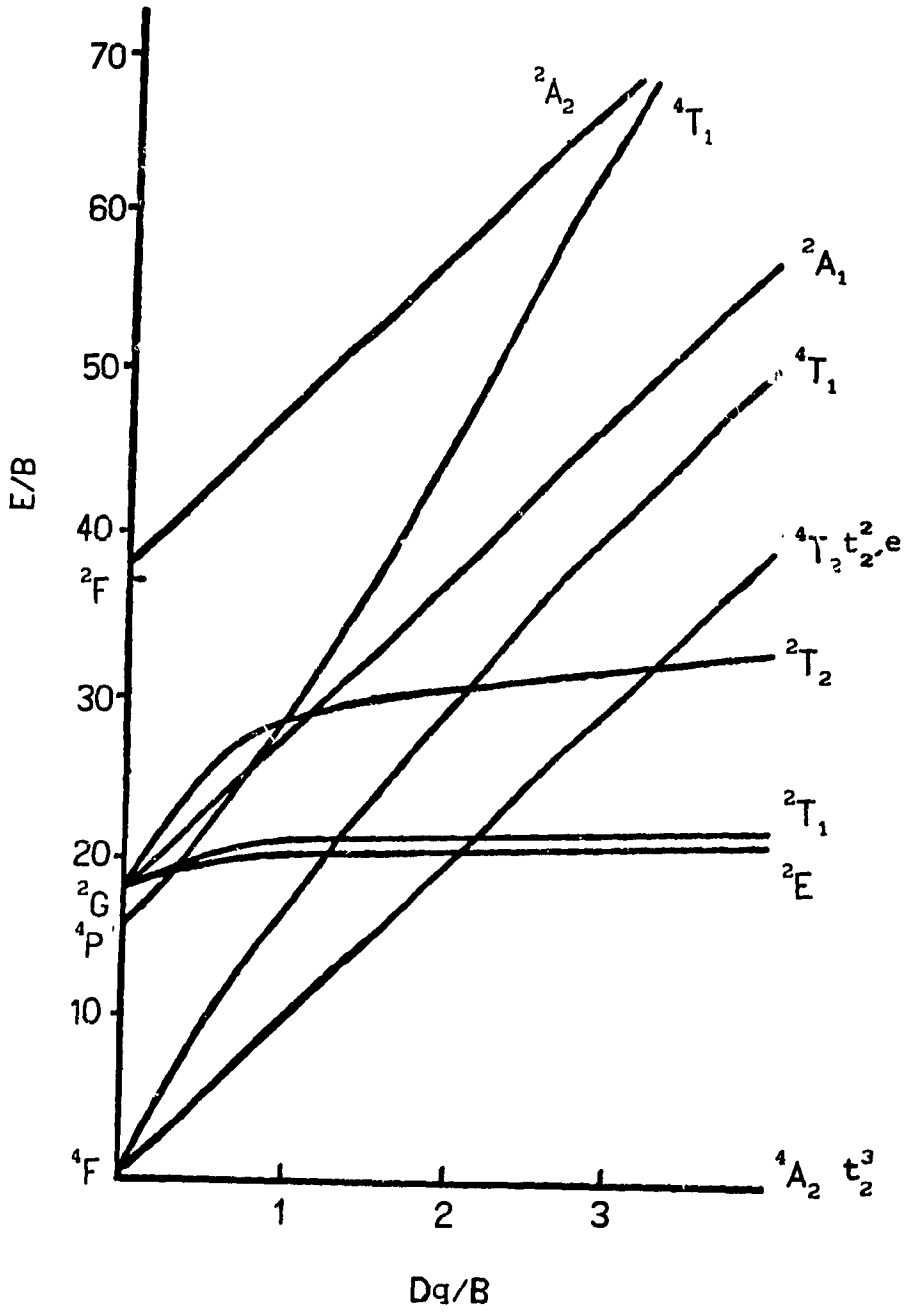

Figure 2.6.3.1 Splitting of the states of the d^3 configuration by an octahedral field.

CHAPTER 3

3. EXPERIMENTAL

3.1 SAMPLE PREPARATION

The sodium in Zeolite X (NaX, Linde Union Carbide) was exchanged for magnesium by treating it with a 40% solution of $MgCl_2$ at 85°C for 10 hours (a fresh solution every 2 hours). The chromium doped cordierite glass NRC-3 ($MgO.Al_2O_3.2.5SiO_2$) was prepared by fusing 6.61 grams of the magnesium exchanged Zeolite (MgX) with 7.3 X 10^{-2} grams of high purity chromium sesquioxide (Johnson Matthey, puratronic 99.99%). Melts were prepared in a platinum crucible and placed in a high temperature electrically heated furnace for 16 hours. The melting and annealing temperatures were 1600°C and 600°C respectively. For annealing, the sample was placed in a furnace for one hour. A schematic outlining the synthesis of the samples is shown in Figure 3.1.1.

A series of chromium doped cordierite based glasses of composition $XMgO.Al_2O_3.2.5SiO_2$ where X = 0.5-2.0 at increments of X = 0.25 were prepared. The mole % of each of these components are listed in Table 3.1.1. The samples NRC-1 and NRC-2 were prepared by fusing silica (SiO_2) magnesium oxide (MgO) and alumina (Al_2O_3) with high purity Cr_2O_3 using the same melting and annealing temperatures as above.

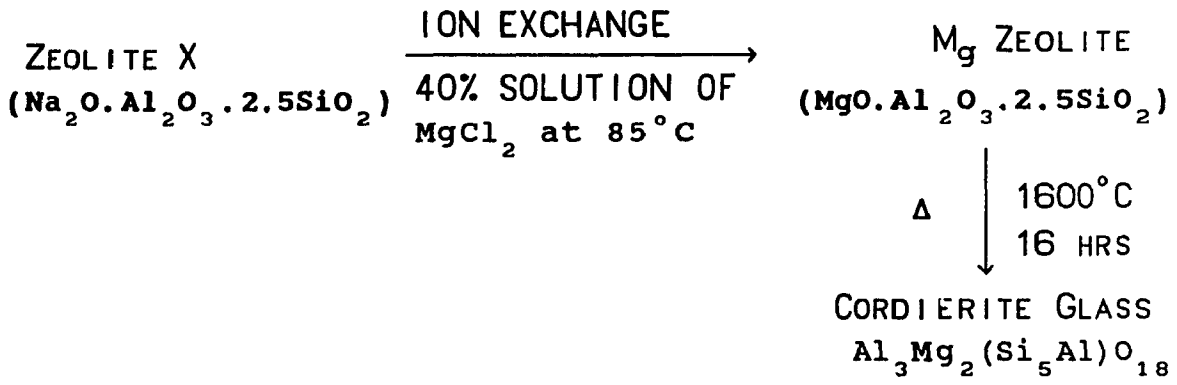

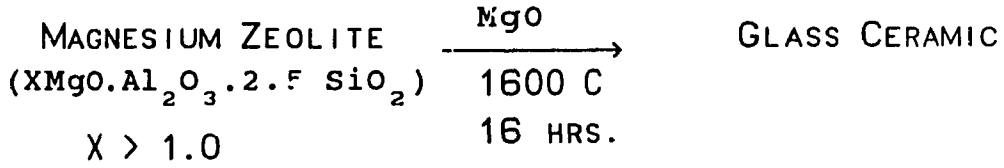

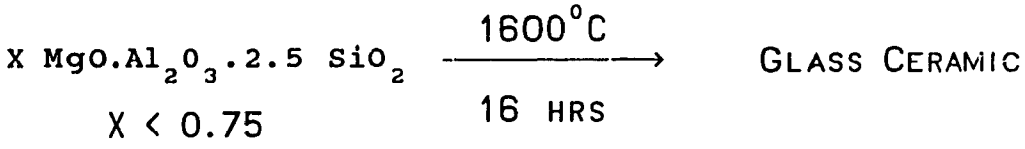

Figure 3.1.1 Flow chart outlining the synthesis of the series $XMgO.Al_2O_3.2.5SiO_2$ where X = 0.5-2.0.

For samples NRC-4 to NRC-7, magnesium exchanged Zeolite X was used as the starting material to which magnesium oxide was added to obtain the desired composition.

TABLE 3.1.1

CORDIERITE SERIES

($XMgO.Al_2O_3.2.5SiO_2$, $0.5 \leq X \leq 2.0$).

SAMPLE	X	GLASS COMPOSITION (MOLE %)			
		SiO_2	MgO	Al_2O_3	Cr_2O_3
NRC-1	0.5	68.40	3.70	27.9	0.05
NRC-2	0.75	65.10	9.10	25.80	0.06
NRC-3	1.0	60.60	16.60	22.80	0.06
NRC-4	1.25	55.30	25.20	19.40	0.07
NRC-5	1.50	54.0	26.70	18.30	0.07
NRC-6	1.75	51.80	31.60	15.50	0.07
NRC-7	2.0	49.20	37.40	13.40	0.06

3.2 OVEN AND TEMPERATURE CONTROLLER

A high temperature air, inert atmosphere furnace (Model 1700S- CM.Inc.Furnaces, Inc. Bloomfield N.J.) was used for fusing and for the application of thermal treatments. The maximum operating temperature is 1700°C. The furnace is powered by a single phase silicon controlled rectifier (SCR) power package (Model 831 Eurotherm Corporation, Virginia).

The SCR is connected to a 220V line and is capable of delivering a maximum current of 75 amps.

3.3 SPECTROSCOPY

3.3.1 ABSORPTION AND EMISSION

Absorption spectra were measured using a Cary 2300 spectrophotometer. Fluorescence spectra were obtained by excitation with a tunable dye laser (Spectra Physics 375) operating with Rhodamine 6G (10^{-3} mol/dm^3 in ethylene glycol) pumped by a coherent Innova 70, 4W argon ion laser operating in the all lines mode.

The spectra were recorded using a Jarrel-Ash 1-m Czerny Turner double monochromator and a maximum slit width of 150 μm. The gratings are mounted on a cosecant bar driven by a stepper motor with a step size of 0.01 cm^{-1}/step.

The emission signal was monitored by an RCA-C31034-02 photomultiplier, which has a flat spectral response from 200 to 850 nm. The photomultiplier was thermoelectrically cooled so that background dark count rate was below 10 counts s^{-1}. The photomultiplier signal is processed by a preamplifier model SR 440 Stanford Research Systems. The preamp contains four wide bandwidth, dc coupled amplifiers designed to be used independently or cascaded to provide gains of 5, 25,

125, and 625 thus amplifying the output from the photomultiplier tube to the photon counter. The Gated Photon Counter Model SR 400 (Stanford Research Systems) is a data acquisition system that interfaces between the computer and the spectroscopic hardware shown in Figure 3.3.1.1. The signal is recorded under computer control using the Stanford SR 465 software data acquisition/analysis system. Some of the data was acquired at liquid nitrogen temperature (77K) using an Oxford Instruments continuous flow cryostat (CF 204).

Time resolved emission spectra and fluorescence lifetime measurements were made with Ar^+/rhodamine 6G laser excitation and a Stanford Research SR 400 gated photon counter. The signal was chopped using a Stanford Research optical chopper, Model SR 450. The photon counter was triggered by a photodiode synchronized by the laser pulse.

3.3.2 HEAT TREATMENT AND CERAMITIZATION OF THE CORDIERITE "MOTHER GLASS"

The first step in the heat treatment for the ceramitization of cordierite glass is to hold the mother glass at a specific temperature for a specified time, in order to induce nucleation. The second step is to raise the temperature for a length of time to promote crystal growth.

The crystallization process can be taken to completion producing a ceramic. This was accomplished by subjecting the cordierite glass doped with 0.17% Cr_2O_3 prepared in the usual manner to a nucleating and crystallizing temperature of 1100°C for 2 hrs and 1250°C for 4-5 hours respectively.

3.3.3 EXCITATION SOURCES

The excitation optical path (Figure 3.3.1.1) consists of mirrors M1 and M2, a focusing lens L1, that collimates the beam to a third mirror (M3), and a spatial filter (NRC model 900) which spatially filters the exciting laser line. The lenses L2 and L3 focus the laser beam onto the sample in the cryostat. Lens (L4) is used to focus the fluorescence signal onto the monochromator slits.

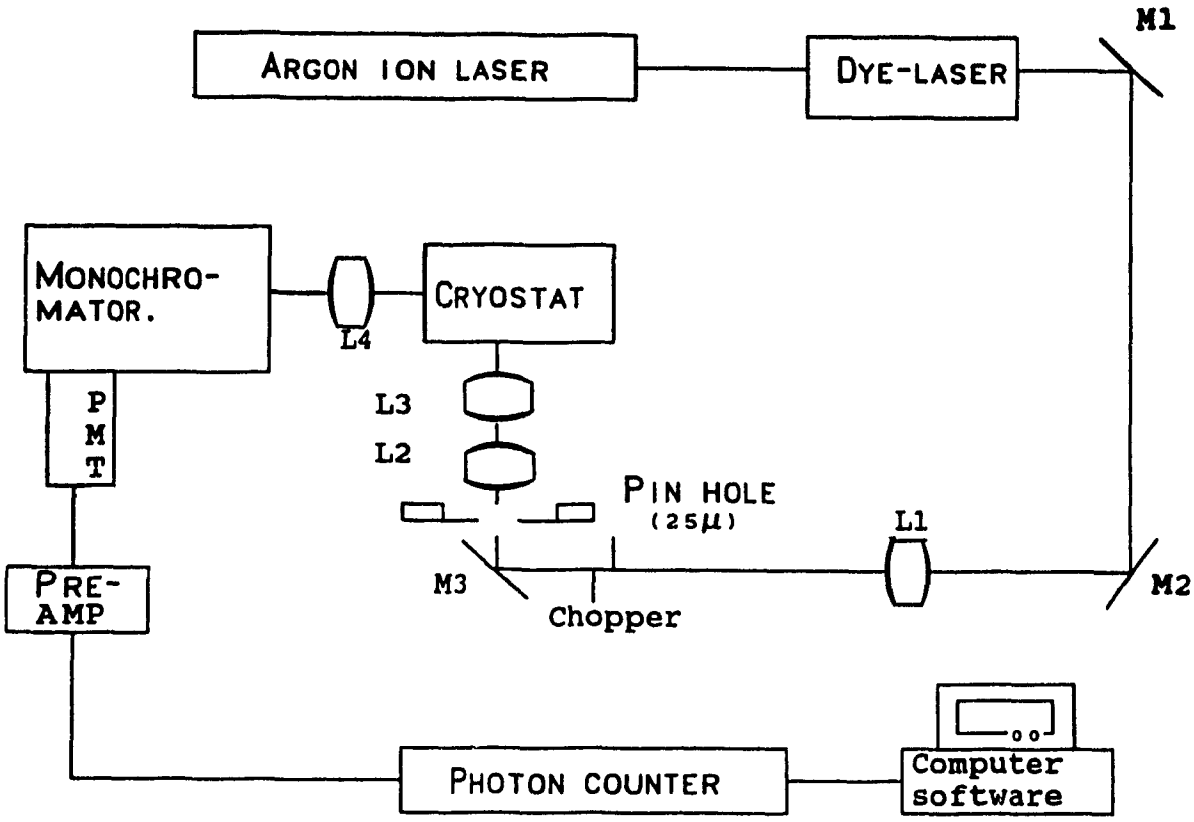

Argon ion Laser:Coherent Innova 70 4W

Dye-laser :Spectra-Physic model 375

Chopper :Stanford optical chopper model SR540

Spatial filter :NRC model 900 (25μ)

Cryostat :Oxford CF-204

Monochromator :Jarrel-Ash 1m Czerny-Turner double monochromator

Photomultiplier :RCA-C31034-02

Pre-Amp. :Stanford fast preamplifier model SR440

Photon Counter :Stanford Gated photon counter model SR400

Figure 3.3.1.1 Schematic arrangement of apparatus for the measurement of emission spectra, time resolved spectra and decay times.

3.4 X-RAY POWDER DIFFRACTION

X-ray powder diffraction was carried out at room temperature on a Philips PW 1050-25 diffractometer, using the Ni-filtered K_α radiation of copper (λ = 1.5417 Å). The samples were contained in a flat holder made of plexiglass for the determination of the Bragg peaks of the ceramics. When checking for the presence of the glass scattering peak, a holder made of aluminum was used. Crushed powdered samples, were packed in a holder, and pressed with a glass plate in order to obtain a smooth flat surface at level with the surface of the holder, for a perfect alignment in the center of the goniometer. For solid bulky samples, a hole slightly larger than the sample was drilled through the plexiglass/Al holder, and the sample was inserted in and held steady in such a way that a smooth flat surface of it was at level with the surface of the holder. The goniometer was rotated at a constant speed of 0.5° (θ)/min and the diffraction pattern was recorded.

3.5 CRYSTAL FIELD CALCULATION

A quantitative crystal field analysis can be made by analyzing the structure of the absorption spectra. One calculates the strong field parameters by diagonalizing the strong field energy matrices of the Coulomb and cubic field operators given by Tanabe and Sugano [36].

The $^4A_{2g}$, $^4T_1$ $^4T_{2g}$, $^2T_{1g}$ and ^2E energy matrices for the d^3 system are given in Table 3.5.1.

TABLE 3.5.1

ENERGY MATRICES FOR SYSTEMS IN AN OCTAHEDRAL FIELD

$^4T_1(^4P, ^4F)$ =

$$\begin{Vmatrix} -2Dq - 3B & 6B \\ & 8Dq - 12B \end{Vmatrix}$$

$^4A_{2g}(^4F) = -12Dq - 15B$

$^4T_{2g}(^4F) = -2Dq - 15B$

$^2E\ (a^2D, b^2D, ^2G, ^2H)$ =

$$\begin{Vmatrix} -12Dq & & & \\ -6B+3C & -6\sqrt{2}B & -3\sqrt{2}B & 0 \\ & -2Dq + 8B+6C & 10B & \sqrt{3}(2B+C) \\ & & -2Dq - B+3C & 2\sqrt{3}B \\ & & & 18Dq - 8B+4C \end{Vmatrix}$$

$^2T_{1g}\ (^2P, ^2F, ^2G, ^2H)$ =

$$\begin{Vmatrix} -12Dq & & & & \\ -6B+3C & -3B & 3B & 0 & -2\sqrt{3}B \\ & -2Dq+3C & -3B & 3B & 3\sqrt{3}B \\ & & -2Dq - 6B+3C & -3B & -\sqrt{3}B \\ & & & 8Dq - 6B+3C & 2\sqrt{3}B \\ & & & & 8Dq - 2B+3C \end{Vmatrix}$$

The eigenvalues E_1, E_2... E_n of these matrices are obtained by solving the corresponding secular or determinantal equations:

$$\begin{Vmatrix} H_{11} - E & H_{12} \cdots\cdots\cdots\cdots\cdots\cdots \\ H_{21} & H_{22} - E \cdots\cdots\cdots\cdots\cdots\cdots \\ \cdots\cdots\cdots\cdots\cdots\cdots\cdots\cdots\cdots\cdots\cdots \\ \cdots\cdots\cdots\cdots\cdots\cdots\cdots\cdots\cdots\cdots\cdots \\ \cdots\cdots\cdots\cdots\cdots\cdots\cdots\cdots & H_{nn} - E \end{Vmatrix}$$

The crystal field parameter Dq was fixed by the $^4T_{2g} \longrightarrow {}^4A_{2g}$ transition in the absorption spectrum of cordierite glass ($Dq = [E(^4T_{2g}) - E(^4A_{2g})]/10$). The Racah parameter B was obtained by substituting the value of Dq into the $^4T_{1g}$ determinantal matrix (Table 3.5.1). Using the ^2E_g transition energy in the emission spectrum, the C parameter was obtained by subsituting the Racah B parameter into the ^2E_g determinantal matrix. The value of the parameter C obtained using the ^2E_g determinantal matrix was compared with the value of the C parameter obtained using the $^2T_{1g}$ transition energy in the absorption spectrum and the $^2T_{1g}$ determinantal matrix.

In calculating the crystal field parameters (Dq, B, C) the energy of the ground state ($^4A_{2g}$) was subtracted from the diagonal entries for each of the determinantal energy matrices ($^4T_{1g}$, ^2E_g, $^2T_{1g}$).

3.6 CALCULATION OF OSCILLATOR STRENGTH

The room temperature extinction coefficients (ε, ℓ mol^{-1} cm^{-1}) were calculated from the absorption data and the glass density. The densities were measured by weighing cut and polished samples of accurately known dimensions. The densities and the extinction coefficient values for the absorption bands ($^4T_{1g}, {}^4T_{2g} \longleftarrow {}^4A_{2g}$) are given in Table 3.6.1.

The oscillator strengths were calculated using equation 3.6.1 [37],

$$f = mc/\pi e^2 \int \sigma(\nu) d\nu \qquad (3.6.1)$$

where m is the mass of an electron, c is the speed of light and e is the electronic charge, and the integrand is the area under the absorption band.

TABLE 3.6.1

DENSITIES OF SAMPLES AND THE EXTINCTION COEFFICIENT VALUES FOR THE ABSORPTION BANDS $^4T_{2g}$, $^4T_{1g} \longleftarrow {}^4A_{2g}$.

SAMPLE	DENSITY ρ $gm\ cm^{-3}$	ε $\ell\ mol^{-1}\ cm^{-1}$	
		$^4T_{2g} \longleftarrow {}^4A_{2g}$	$^4T_{1g} \longleftarrow {}^4A_{2g}$
NRC-1	2.43	8.49	13.40
NRC-2	2.37	11.37	14.92
NRC-3	2.00	17.15	26.57
NRC-4	2.19	9.92	16.23
NRC-5	2.37	5.61	9.84
NRC-6	2.70	5.46	9.78
NRC-7	2.21	3.33	7.08

CHAPTER 4

4. RESULTS AND DISCUSSION

4.1 THE STRUCTURE OF CORDIERITE GLASS (MAGNESIUM ALUMINO-SILICATE).

The choice of glass composition for this thesis is cordierite $MgO.Al_2O_3.2.5SiO_2$. Cordierite was chosen because of its high optical quality and superior mechanical durability. As shown in Table 4.1.1 the glass ceramic phase of cordierite possesses a bending strength approximately 2 times higher than most oxide glasses [38].

TABLE 4.1.1

BENDING STRENGTH OF VARIOUS TYPES OF GLASS CERAMIC MATERIALS.

GLASS SYSTEM	MAIN CRYSTALLINE PHASE	BENDING STRENGTH (MPA)	
		GLASS	GLASS CERAMIC
SiO_2-Li_2O	$SiO_2.Li_2O$ $SiO_2.2Li_2O$	80	150
SiO_2-Al_2O_3-Li_2O	β-SPODUMENE S.S.	110	180
SiO_2-Al_2O_3- MgO	CORDIERITE	150	300
SiO_2-Al_2O_3- CaO	WOLLANSTONITE	70	130
SiO_2-Al_2O_3- ZnO	GAHNITE	60	110
SiO_2-Al_2O_3- MgO-K_2O-F	FLUOROPHOGOPITE	80	105

The basic unit, or the glass forming species in cordierite is SiO_4. The ratio of the radius r_{Si} to r_O is about 0.30. As shown in Table 4.1.2 such a ratio implies a tetrahedral arrangement [39]. The tetrahedral arrangement is also favored by the bonding electrons in SiO_2, since silicon may be sp^3 hybridized and these orbitals may interact with the p orbitals of the oxygen. Figure 4.1.1a shows a two dimensional representation of the silica network in the glass [39].

TABLE 4.1.2.

RADIUS RATIO AND COORDINATION REQUIREMENTS IN POLYHEDRA OF DIFFERENT GEOMETRIES.

RADIUS	COORDINATION	POLYHEDRON
0.155 - 0.225	3	TRIANGLE
0.225 - 0.414	4	TETRAHEDRON
0.414 - 0.732	6	OCTAHEDRON
0.732 - 0.904	8	HEXAHEDRON, CUBE
> 0.904	12	ICOSAHEDRON

Another constituent in cordierite glass is magnesium oxide. Magnesium is a network modifying cation, and is accommodated randomly in the network in close proximity to nonbridging oxygens. The nonbridging oxygens are created since the modifier, (Mg in cordierite), disrupts the otherwise perfectly connected random network.

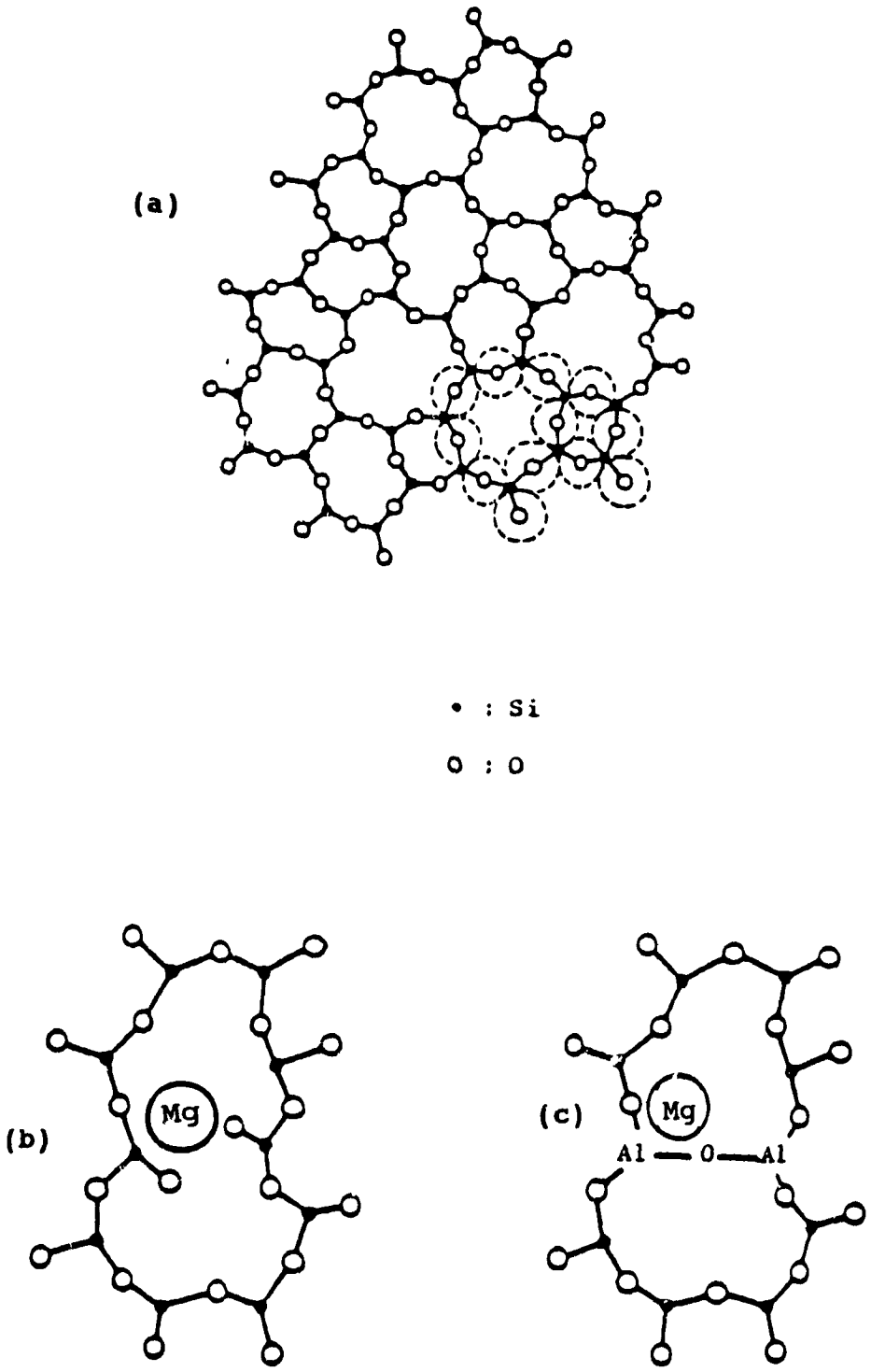

Figure 4.1.1 A two dimensional representation of the ternary glass system SiO_2-Al_2O_3-MgO.

The difference between a bridging and nonbridging oxygen is shown schematically as follows;

$$(=Si-O-Si=) + (MgO) \longrightarrow (=Si-O--Mg--O-Si=) \quad (4.1.1)$$

where the arrangement (Si—O—Si) shows a bridging oxygen, by contrast to a nonbridging oxygen (O--Mg--O). The structure at this point is shown in Figure 4.1.1 b.

Alumina, Al_2O_3, the third and final constituent of cordierite, is of secondary importance in terms of its glass forming ability. It is recognized as an intermediate glass former since Al^{3+} can replace Si^{4+} substitutionally or it can be found interstitially. The ratio of the radius of Al^{3+} to oxygen is 0.43, therefore it can be either in a four or six coordination environment (Table 4.1.2). The coordination that Al^{3+} will assume depends upon the glass structure. There are two cases to consider. If Al_2O_3 is added to a pure silica glass, the Al^{3+} ion would be forced to assume six coordination $(AlO_6)^{3-}$ since the tetrahedral bonding in pure silica is very stable and not easily substituted. In this case the Al^{3+} ion acts as a modifier. However, due to the presence of nonbridging oxygens introduced by MgO in cordierite, the O^{2-} ions are not as tightly bound thereby allowing the possibility of a four coordinated Al^{3+} ion $(AlO_4)^-$ by substituting for Si^{4+}. The cordierite glass consists of an infinite chain of edge shared AlO_6 octahedral cross linked by AlO_4 and SiO_4 tetrahedra (Figure 4.1 1 c).

4.2 CHROMIUM SITES IN THE CORDIERITE GLASS STRUCTURE

The infinite chain of edge shared AlO_6 octahedral cross linked by AlO_4 and SiO_4 tetrahedra in cordierite glass provide two ways in which the Cr^{3+} ion can exist in the glass structure; (a) as a modifier, where the environment of the Cr^{3+} ion is determined by the glass structure, or (b) as a network former by substitution into the network sites. As a modifier, the open structure in cordierite glass provides polyhedra large enough to accommodate the activator ion interstitially. As a network former, the octahedral bonding requirements of Cr^{3+} can be satisfied if Cr^{3+} replaces the octahedrally coordinated Al^{3+} substitutionally.

4.3 SPECTROSCOPY OF CHROMIUM (III) IN CORDIERITE

4.3.1 ABSORPTION AND EMISSION IN THE CORDIERITE MOTHER GLASS

For the Cr^{3+} ion, luminescence originates from transitions in the unfilled 3d electronic shell. The designations of the transitions for Cr^{3+} in octahedral symmetry are shown in Figure 4.3.1.1 [34].

The optical absorption and emission spectra of the cordierite mother glass (NRC-3) at liquid helium temperature are shown in Figure 4.3.1.2a,b respectively.

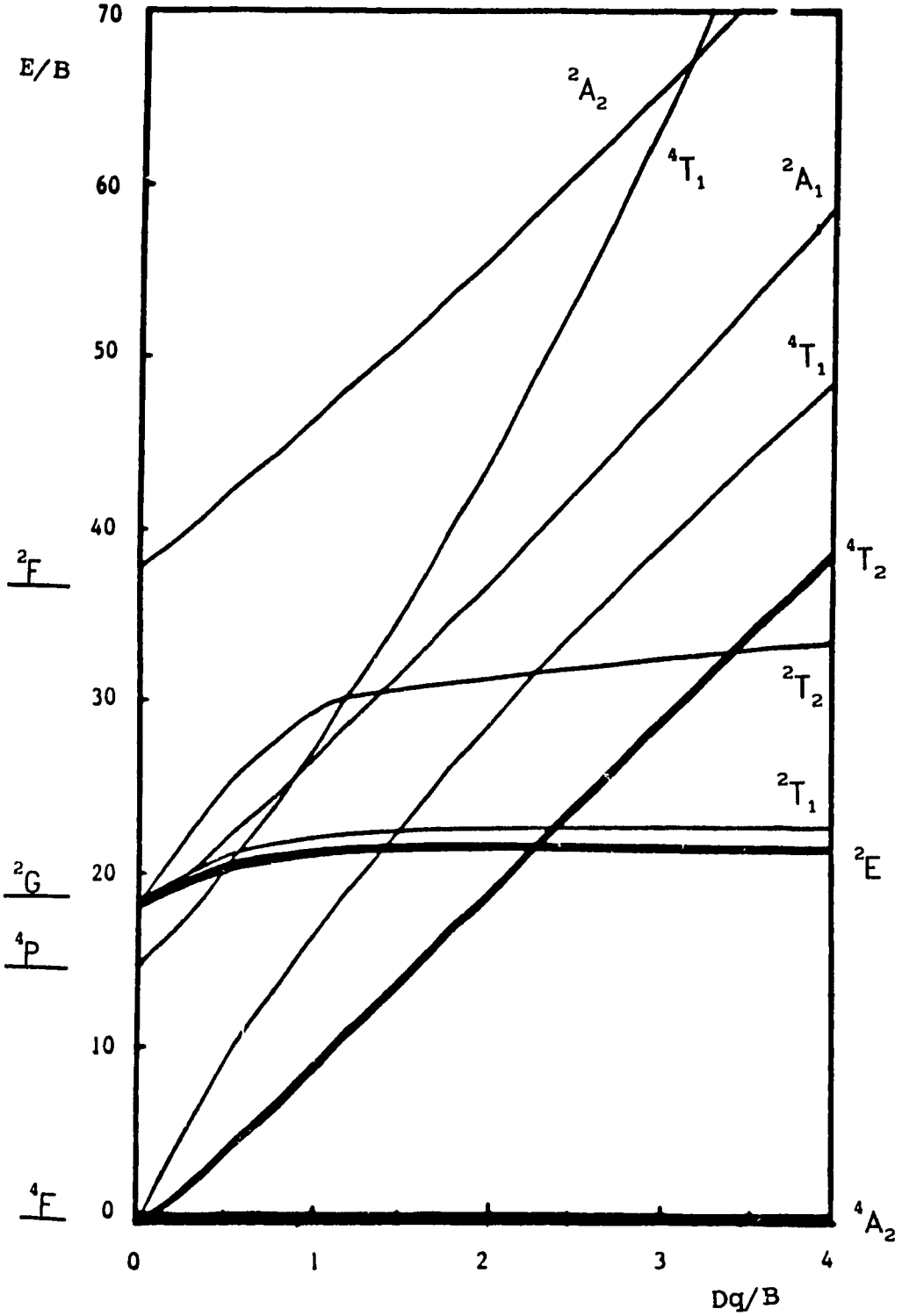

Figure 4.3.1.1 Tanabe and Sugano energy level diagram for the d^3 configuration in octahedral coordination.

The principal features of the absorption spectrum (Figure 4.3.1.2a) are two broad bands with maxima at 15180 cm^{-1}(658 nm) and 22279 cm^{-1} (449 nm) which are assigned to the vibronically broadened transition $^4T_{2g}(t_{2g}^2 e_g) \longleftarrow {}^4A_{2g}(t_{2g}^3)$ and $^4T_{1g}(t_{2g}^2 e_g) \longleftarrow {}^4A_{2g}(t_{2g}^3)$ respectively. An interesting feature in the absorption spectrum is the fine structure in the $^4T_{2g} \longleftarrow {}^4A_{2g}$ transition. The absorption minimum at 14275 cm^{-1} (Figure 4.3.1.2 a) can be assigned to the $^2E_g \longleftarrow {}^4A_{2g}$ transition on the basis that it overlaps exactly with the $^2E_g \longrightarrow {}^4A_{2g}$ transition of the emission spectrum (Figure 4.3.1.2 b). The other minimum at 15259 cm^{-1} (Figure 4.3.1.2 a) can be assigned to the $^2T_{1g} \longleftarrow {}^4A_{2g}$ transition. These transitions are interpreted as Fano antiresonance [40] and the transition energies are assigned to the minima rather than to the spectral peaks . The Fano antiresonance can be explained in terms of a spin orbit interaction that takes place between two energy levels that are isoenergetic such as the discrete ^2E_g or $^2T_{1g}$ energy level and the $^4T_{2g}$ continuum. The observed dips arise from the forbidden transition due to the mixing of states.

4.3.1.1 INHOMOGENEOUSLY BROADENED LINE WIDTHS

A qualitative, but significant aspect of the absorption spectrum is the bandwith at half maximum (BWHM) or in short, the halfwidth. The halfwidth gives a measure of site distribution of the activator ion within the host material.

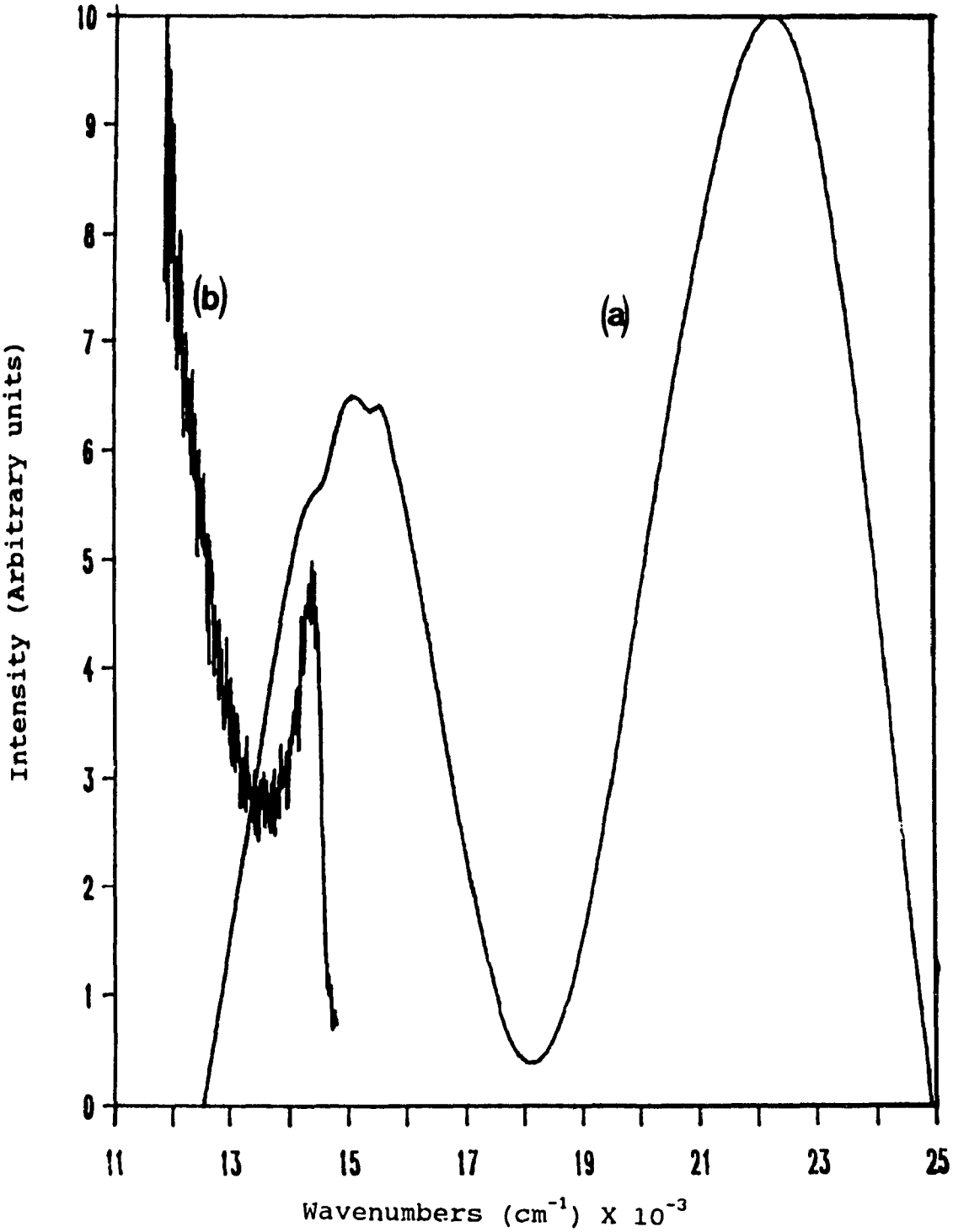

Figure 4.3.1.2 Liquid helium absorption (a) and emission spectra (b) of Cr^{3+} in sample NRC-3 (mother glass)

Glass is amorphous and epitomizes an inhomogeneous system. The environment of "each ion" in the glass is different. Therefore there exists a wide distribution of local crystal fields between individual ion sites. This gives rise to site to site differences in the energy levels of the activator ion in the glass. The Cr-O interatomic distances vary about an average value, with distorted symmetries, as shown in Figure 4.3.1.1.1. This means that the energy separation and the order of the emitting states ($^4T_{2g}$ and ^2E_g) varies from site to site. The halfwidth is in fact a superposition of contributions from individual ions distributed among an entire ensemble of local environments.

The $^4T_{2g} \longleftarrow {}^4A_{2g}$ transition at 15180 cm^{-1} in the absorption spectrum (Figure 4.3.1.2) was estimated to have a halfwidth of 3433 cm^{-1}. This value is comparable to most chromium doped oxide glasses. For comparative purposes the halfwidths of the $^4T_{2g} \longleftarrow {}^4A_{2g}$ band for some oxide glasses, glass ceramics, and crystals at room temperature are listed in Table 4.3.1.1.1.

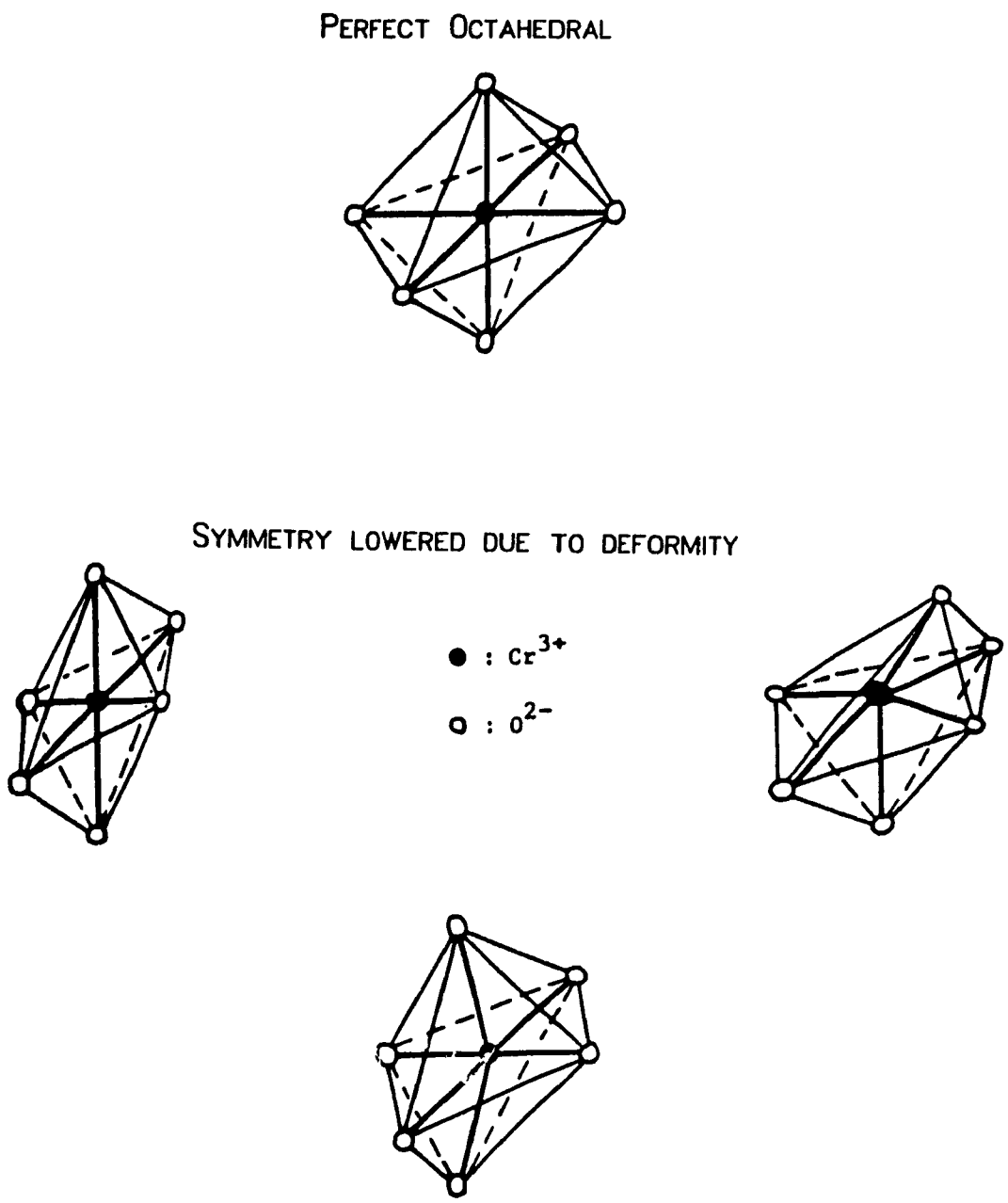

Figure 4.3.1.1.1 Schematic diagram showing some possible octahedral sites within the host material.

TABLE 4.3.1.1.1

HALFWIDTHS OF THE $^4T_{2g}$ ABSORPTION BAND IN SOME CHROMIUM DOPED HOST MATERIALS.

HOST	HALFWIDTH (cm^{-1})	REFERENCE
GLASS		
CORDIERITE	3433	this work
SODA LIME GLASS	3500	[41]
PHOSPHATE	3800	[41]
CRYSTAL		
$LiCaAlF_6$	200	[42]
$Be_3Al_2(SiO_3)_6$ (emerald)	795	[43]
$BeAl_2O_4$ (alexandrite)	1150	[44]
GLASS CERAMIC		
$3Al_2O_3.2\ SiO_2$ (mullite)	1600-2600	[45]

4.3.1.2 EMISSION IN CORDIERITE GLASS

The spectral features of fluorescence and phosphorescence in the samples studied can be interpreted with the aid of the simplified Tanabe-Sugaro diagram for d^3 ions in an octahedral field shown in Figure 4.3.1.2.1.

One can distinguish three distinct fields; the high field to the right of the crossover point, an intermediate field near the crossover point and the low field to the left handside

of the crossover point.

Figure 4.3.1.2.2 shows the emission spectrum of cordierite glass NRC-3 at liquid nitrogen temperature excited at 572 nm. The spectrum consists of two broad bands centered at 820 and 692 nm. These bands can be assigned to the $^4T_{2g} \longrightarrow {}^4A_{2g}$ and $^2E_g \longrightarrow {}^4A_{2g}$ transitions respectively. The presence of these two bands indicates that the Cr^{3+} ions are found in an intermediate field and the zero phonon $^4T_{2g}$ level is nearly isoenergetic to the ^2E_g electronic manifold. This situation is depicted schematically in Figure 4.3.1.2.1c.

It is worth noting at this point that the halfwidth of the $^4T_{2g}(t_{2g}^2 e_g) \longrightarrow {}^4A_{2g}(t_{2g}^3)$ transition at 820 nm (BWHM=1055 cm^{-1}) is about 2.5 times larger than the halfwidth for the $^2E_g(t_{2g}^3) \longrightarrow {}^4A_{2g}(t_{2g}^3)$ transition at 706 nm (BWHM= 410 cm^{-1}) shown in Figure 4.3.1.2.2 . This can be explained in the following way.

During absorption of radiation, an electron is promoted from the ground $^4A_{2g}(t_{2g}^3)$ energy level to an e_g orbital of the excited electronic state $^4T_{2g}(t_{2g}^2 e_g)$. This results in an increased electrostatic repulsion in the excited state, since the e_g orbitals are pointed along the axes of the octahedron, at the ligands.

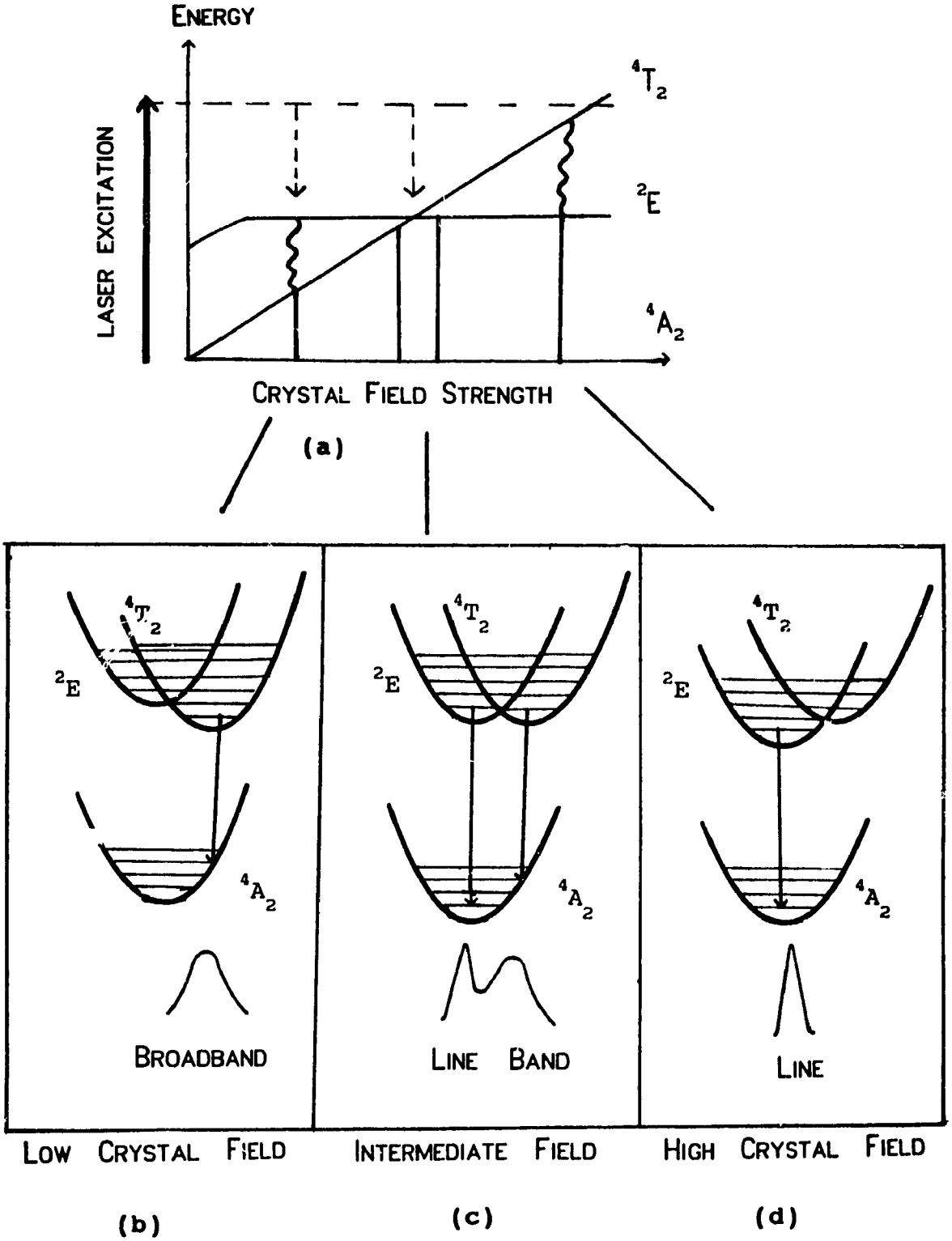

Figure 4.3.1.2.1 The simplified Tanabe-Sugano diagram showing the configuration coordinate diagram of Cr^{3+} energy levels in the three cases shown schematically.

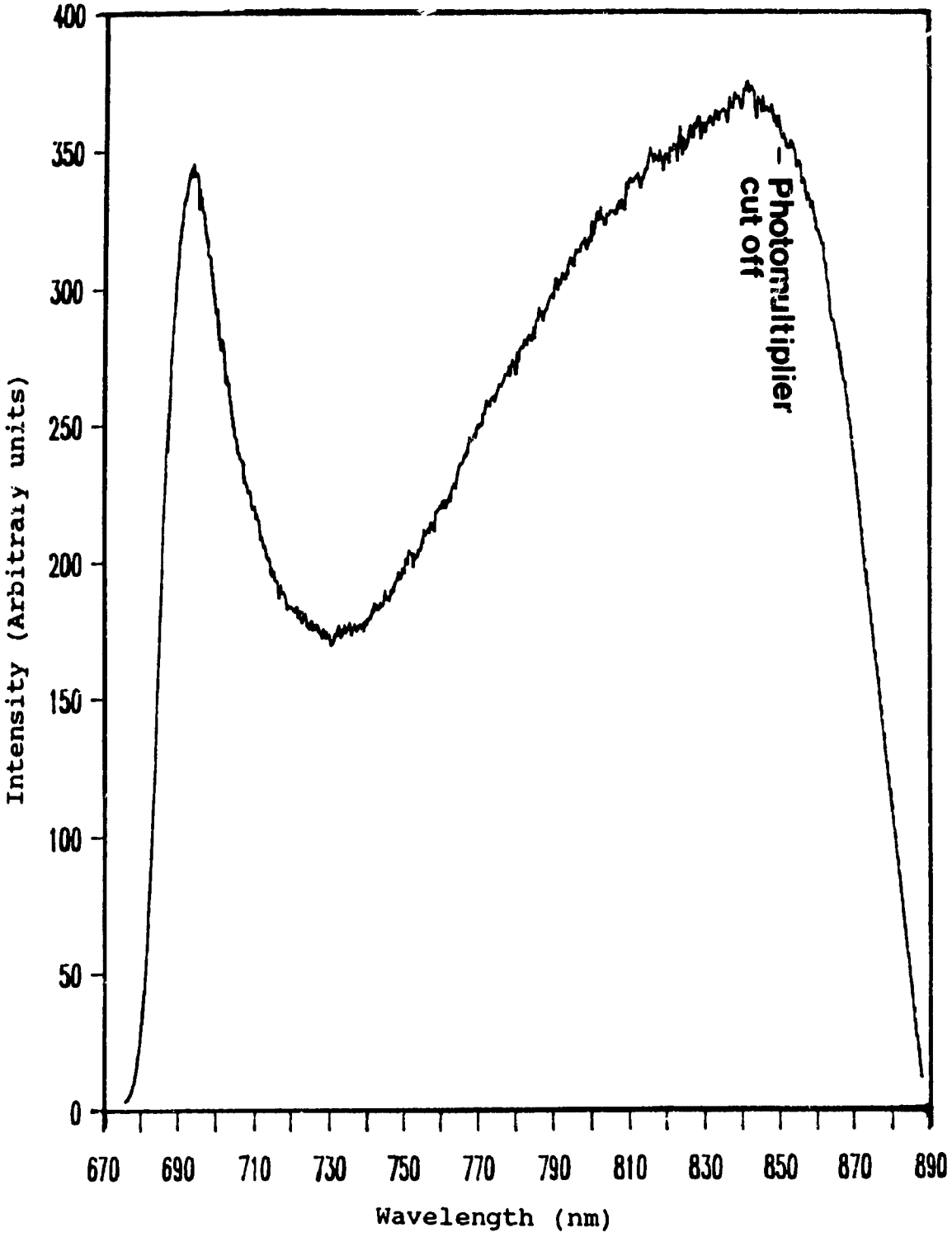

Figure 4.3.1.2.2 Emission spectrum of cordierite glass NRC-3 at 77 K excited at 572 nm.

Therefore one would expect that this will result in a distorted geometry in the excited state, and an increase of the equilibrium distance between Cr^{3+} and the ligands. The band width is proportional to the slope of the energy level curve as a function of the intermolecular distance, taken at the equilibrium point of the ground state [46] . This distortion is the major cause of the observed "broad" band. The situation is depicted schematically in Figure 4.3.1.2.1c.

The relatively sharp $^2E_g \longrightarrow {}^4A_{2g}$ transition centered at 692 nm shown in Figure 4.3.1.2.2 can be explained in a similar manner. The reason for the sharper transition lies in the fact that both the ground state $^4A_{2g}$ and the excited state ^2E_g arise from the lower set of d orbitals t_{2g}^3, where the lobes point between the ligands thus minimizing the electrostatic repulsion. Consequently, the equilibrium distance between Cr^{3+} and its ligands remain nearly unaltered.

The interpretation of the absorption spectrum (Figure 4.3.1.2) was based on transitions associated with Cr^{3+} in an octahedral envirnoment. This is justified in terms of the ligand field stabilization energy of Cr^{3+}. In an octahedral aquocomplex, it has a value of 258.8 KJ/mole which is approximately 5 times greater than the corresponding stabilization energy for Cr^{3+} in a tetrahedral field [47].

However there is also evidence that suggests that the octahedral coordination is preferred by Cr^{3+} in most oxide glass systems. Zarzycki [48], has determined the coordination number and color for d^n ions ranging from n = 1 to 9 in various vitreous host materials in terms of their crystal field shown in Table 4.3.1.2.1. Furthermore, the value of the ionic ratio of Cr^{3+} with respect to the oxide ligand is;

$$\frac{r_c}{r_a} = \frac{0.63}{1.32} = 0.48 \qquad (4.3.1.2.1)$$

where c = cation, and a = anion. As shown in Table 4.1.2 this ratio also suggests a coordination number of 6 for chromium (III).

In addition, Bamford [49], Bates [50], and Tisher [51], studied the effects of compositional changes and hydrostatic pressure on Cr(III) absorption in silicate glasses, and concluded that the Cr(III) sites are surrounded by six oxygens with an approximate cubic symmetry.

TABLE 4.3.1.2.1

COORDINATION OF TRANSITON METAL IONS DETERMINED ACCORDING TO LIGAND FIELD THEORY C.N.* = COORDINATION NUMER.

ELECTRONIC CONFIGURATION	ION	TYPE OF GLASS	C.N.*	COLOR
$3d^1$	Ti^{3+}	PHOSPHATES	6	VIOLET BROWN
	V^{4+}	BOROSILICATE SILICATES	6	BLUE
$3d^2$	V^{3+}	SILICATES, BORATES, PHOSPHATES BORO-SILICATES	6	GREEN
$3d^3$	Cr^{3+}	SILICATES, BORATES ALUMINOPHOPHATES	6	LIGHT-GREEN
	V^{2+}	SILICATES, ALUMINO-PHOSPHATES	6	
$3d^4$	Mn^{2+}	SILICATES, BORATES	6	VIOLET
$3d^5$	Mn^{2+}	SILICATES	4 OR 6	PALE YELLOW
	Fe^{3+}	SILICATES, BORATES	4 OR 6	BROWN
$3d^6$	Fe^{2+}	SILICATES, BORATES, ALUMINOPHOSHATES	4 OR 6	BLUE GREEN
$3d^7$	Co^{2+}	ALKALINE RICH BORATES	4	BLUE
		ALKALINE POOR BORATES	6	ROSE
		SILICATES	4	BLUE
$3d^8$	Ni^{2+}	ALKALINE RICH BORATES	4	BLUE
		ALKALINE POOR BORATES	6	YELLOW
		SILICATES, ALMINO-PHOSPHATES	4	
$3d^9$	Cu^{2+}	SILICATES, BORATES ALUMINOPHOPHATES	6	BLUE

4.3.1.3 CALCULATION OF THE CRYSTAL FIELD PARAMETERS

The crystal field parameters, were obtained by solving the Tanabe Sugano matrices for the strong field approximation [36]. From the room temperature absorption spectrum (Figure 4.3.1.2) the crystal field parameters Dq and B are fixed by the $^4T_{2g} \longleftarrow {}^4A_{2g}$ $^4T_{1g} \longleftarrow {}^4A_{2g}$ positions, respectively. From the emission maximum of the ^2E_g level (Figure 4.3.1.2.2), the C parameter was obtained. The energies for cordierite glass (NRC-3) are: Dq = 1582 cm^{-1}, B = 781 cm^{-1}, C/B = 3.98 cm^{-1}, (Dq/B = 2.3). The value obtained for the ratio of the crystal field parameter Dq to the Racah parameter B (Dq/B = 2.3) in cordierite glass (NRC-3) is not surprising. The emission spectrum of cordierite glass (NRC-3, Figure 4.3.1.2.2) consists of a broad band centered at 820 nm and a sharper band at 690 nm. The broadband was assigned to $^4T_{2g} \longrightarrow {}^4A_{2g}$ fluorescence whereas the sharper feature was assigned to $^2E_g \longrightarrow {}^4A_{2g}$ R-line phosphorescence. As shown in the simplified Tanabe Sugano diagram (Figure 4.3.1.2.1c) the two emission bands occur at or near the crossover point, where the ratio Dq/B $\cong$ 2.3. Furthermore, The ratio of C/B corresponds very closely to that obtained for other chromium doped oxide glass systems in an intermediate crystal field environment [52].

As an alternative mean of classifying materials and connecting the nature of the emission band to the ligand field, Kenyon [53] introduced the parameter δ. This parameter represents the energy difference between the ^2E_g state and the zero phonon $^4T_{2g}$ energy level [$\delta = E(^4T_{2g}) - E(^2E_g)$]. The value estimated for the cordierite glass (NRC-3) is -806 cm^{-1}. This implyies that the $^4T_{2g}$ energy level lies below the ^2E_g state. Table 4.3.1.3.1 shows the relation between δ and the ratio Dq/B.

TABLE 4.3.1.3.1

CLASSIFICATION OF MATERIALS IN TERMS OF THE PARAMETER DELTA AND ITS RELATION TO THE RATIO Dq/B.

High Field	**Dq/B > 2.3**	**δ > 0**	**sharp line emission**
Intermediate Field	**Dq/B ≃ 2.3**	**δ ≃ 0**	**mixture of sharp and broad emission (fluorescence and phosphorescence)**
Low Field	**Dq/B < 2.3**	**δ < 0**	**broadband emission (fluorescence)**

Table 4.3.1.3.1 shows that cordierite glass (NRC-3) is a low field host material and that its emission spectrum should consist only of a broad band fluorescence due to the $^4T_{2g} \longrightarrow {}^4A_{2g}$ transition since δ < 0. The emission spectrum of cordierite glass (Figure 4.3.1.2.2) however reveals the presence of two bands arising from the $^2E_g \longrightarrow {}^4A_{2g}$ and $^4T_{2g} \longrightarrow {}^4A_{2g}$ transitions at 692 and 820 nm respectively.

This anomaly can be resolved by comparing cordierite glass with other hosts by plotting Dq as a function of δ. [54]. Figure 4.3.1.3.1 shows the variation of Dq as a function of δ for a wide range of materials. The straight line is derived from the approximation that the energy separation of the $^4T_2$ state from the ^2E is a linear function of 10Dq assuming that Racah parameters B and C are constant. Assuming that this relationship holds for glasses, the value of Dq versus δ for cordierite glass (NRC-3) is placed on Figure 4.3.1.3.1. The placement of cordierite glass appears to be correct. It is close to $LiNbO_3$ and and K_2NaScF_6, materials of low to intermediate crystal field that have halfwidths of 1062 and 1017 cm^{-1} respectively.

4.3.1.4 THERMALIZATION EFFECT IN THE EMISSION OF CORDIERITE GLASS

Figure 4.3.1.4.1a,b shows the emission spectrum of the cordierite mother glass (NRC-3) taken at room and at liquid nitrogen temperatures respectively.

It is immediately apparent that there are significant spectral changes which accompany the change in temp-erature. The room temperature emission spectrum shown in Figure 4.3.1.4.1a is characterized by a broaband centered at 780 nm and a shoulder of weaker intensity at 690 nm that can be assigned to the $^4T_{2g} \longrightarrow {}^4A_{2g}$ and $^2E_g \longrightarrow {}^4A_{2g}$ transition respectively.

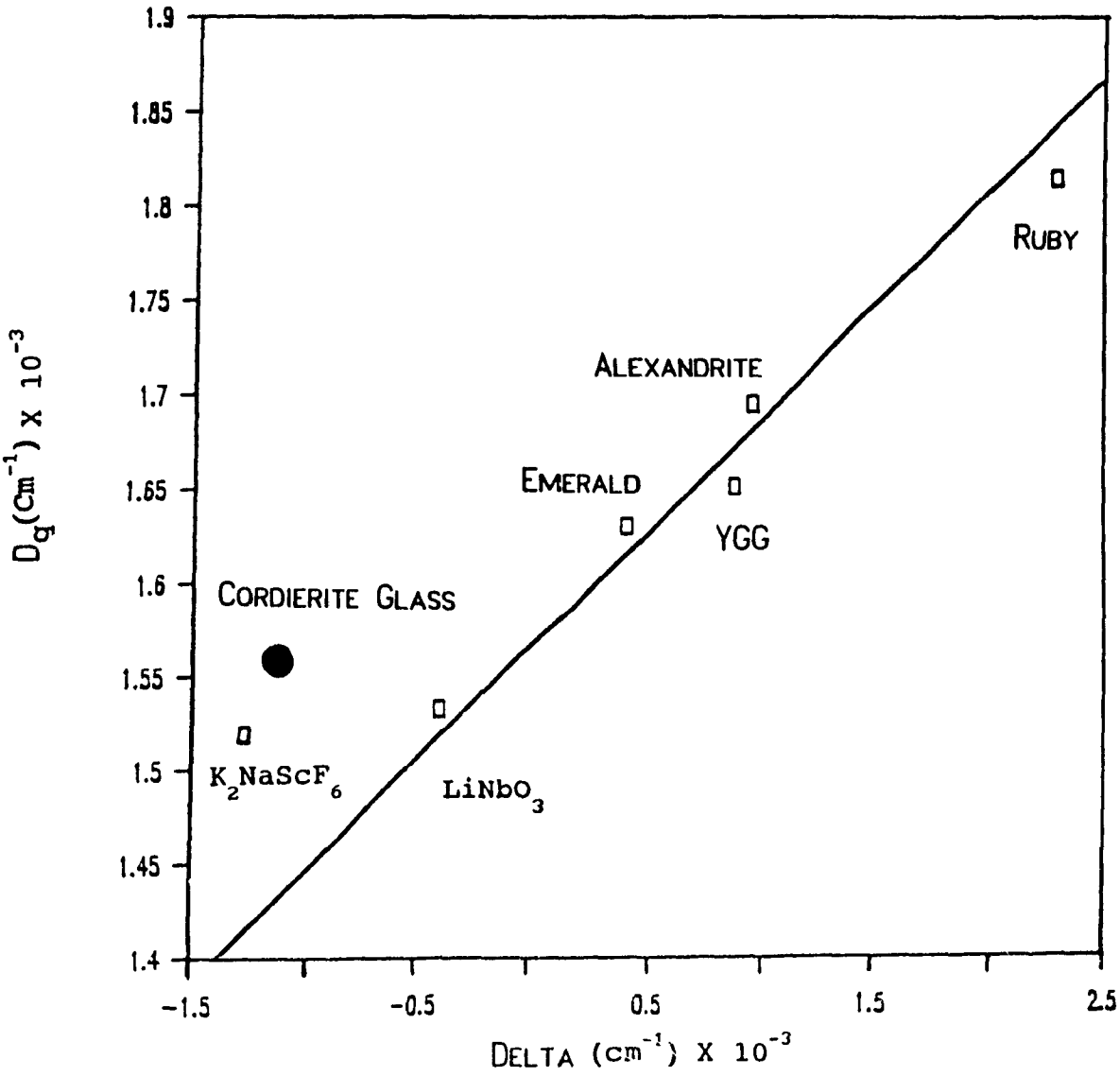

Figure 4.3.1.3.1 Dq versus Delta (δ) for a series of Cr:doped hosts including cordierite (NRC-3).

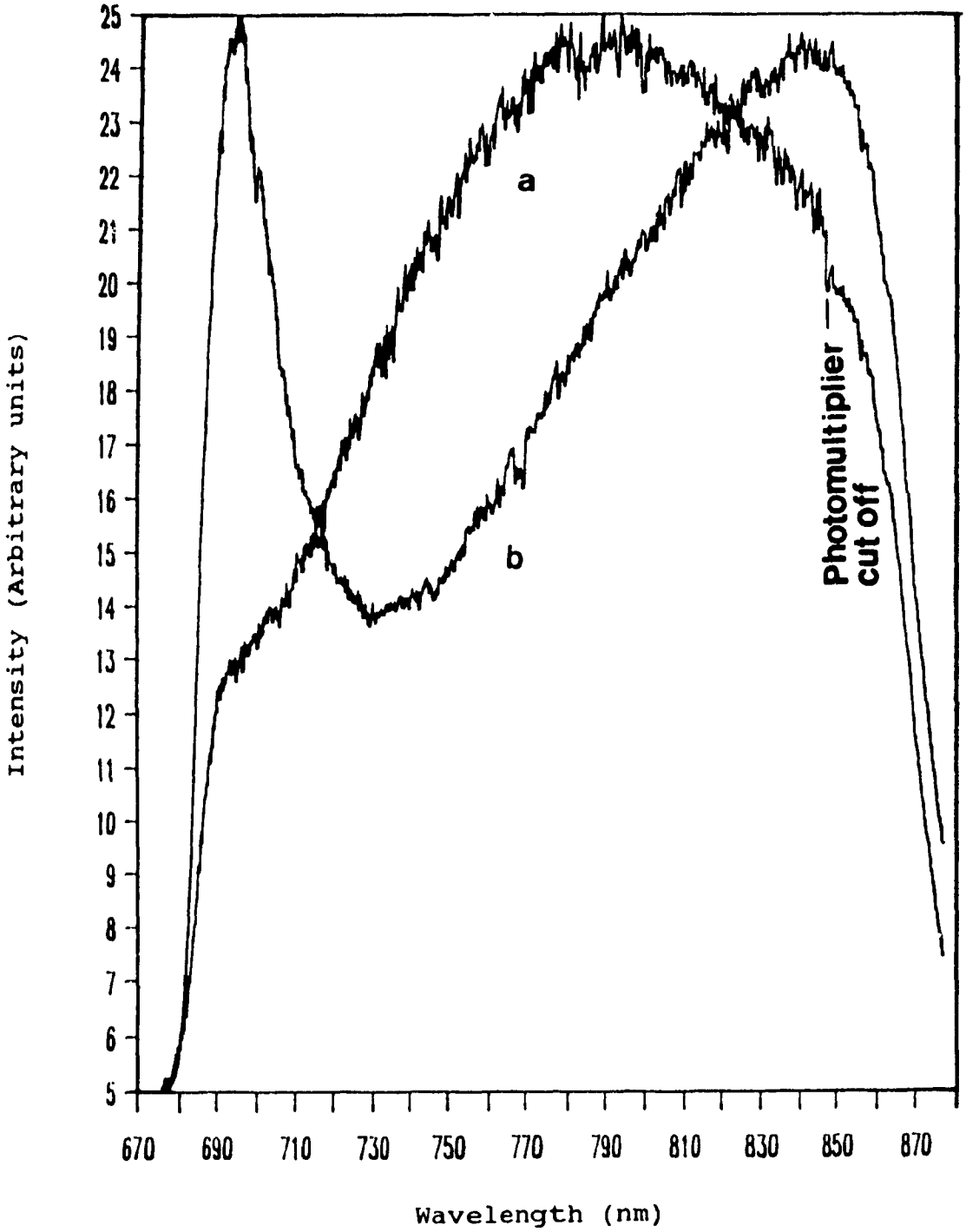

Figure 4.3.1.4.1 Emission spectra of cordierite glass NRC-3 at room temperature (a) and 77K (b) excited at 572 nm.

At 77 K the $^4T_{2g} \longrightarrow {}^4A_{2g}$ transition is displaced towards lower energy and is centered at approximately 840 nm and the $^2E_g \longrightarrow {}^4A_{2g}$ transition (690 nm) is more intense (Figure 4.3.1.4.1b). The spectral changes are due to the thermalization effect. The increase in the band intensity of $^2E_g \longrightarrow {}^4A_{2g}$ transition at 77K can be explained in the following way.

Figure 4.3.1.4.2 shows the three level system present in chromium (III)

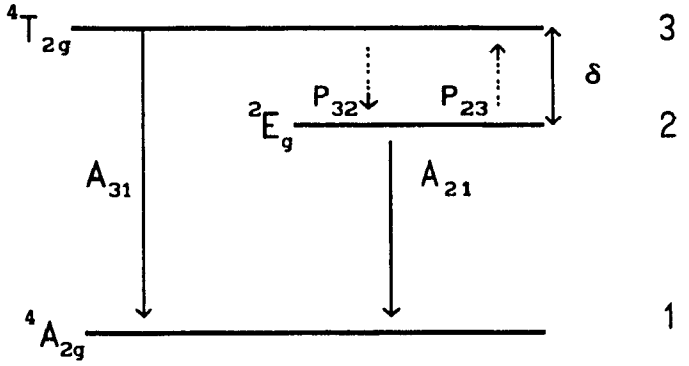

Figure 4.3.1.4.2 A schematic representation of the energy level scheme in chromium (III).

The number of photons emitted from each level ($^4T_{2g}$ and ^2E_g) based on a kinetic model for a three level scheme is given by Equation 4.3.1.4.1 [55].

$$\frac{N\,(^4T_{2g} \longrightarrow {}^4A_g)}{N\,(^2E_g \longrightarrow {}^4A_g)} = \frac{P_{32}\,A_{31}\,EXP(-\delta/KT)}{A_{21}(P_{32} + A_{31})} \qquad (4.3.1.4.1)$$

where $N(^4T_{2g} \longrightarrow {}^4A_{2g})$ and $N(^2E_g \longrightarrow {}^4A_{2g})$ are the number of photons emitted from the $^4T_{2g}$ and ^2E_g excited states respectively. A_{31} and A_{21} are the emissive probability of the excited state, P_{32} and P_{23} are the non radiative probabilities and $A_{31} >> A_{21}$.

The position of the $^4T_{2g} \longrightarrow {}^4A_{2g}$ and $^2E_g \longrightarrow {}^4A_{2g}$ transitions are directly related to the thermally equilibrated excited states ^2E_g and $^4T_{2g}$. According to Equation 4.3.1.4.1 the $^4T_{2g} \longrightarrow {}^4A_{2g}$ transition predominates at high temperatures, whereas the $^2E_g \longrightarrow {}^4A_{2g}$ transition predominates at liquid nitrogen temperature. Furthermore, the sharper linewidth of the $^2E_g \longrightarrow {}^4A_{2g}$ transition (Figure 4.3.1.4.1b) can be attributed to a weaker vibronic coupling between the ^2E_g and the $^4T_{2g}$ excited states that occurs when the temperature is reduced (77K).

Using the semiclassical model [56] to explain line shapes arising from the interaction of the electronic states with the vibrational modes of the crystal, one can account for i) the shift of the $^4T_{2g} \longrightarrow {}^4A_{2g}$ transition towards lower energy at 77K (Figure 4.3.1.4.1b) and ii) the increase in the band intensity of $^2E_g \longrightarrow {}^4A_{2g}$ transition at 77K (Figure 4.3.1.4.1b).

The semiclassical approximation for linear interaction according to Kiel [56] is given by,

$$I_{a,b}(E) = \left[\frac{\tanh(\hbar\omega/2kT)}{\pi(a\hbar\omega)^2}\right]^{1/2} \mathrm{Exp}\left[-(E - E_{ab})^2 . \frac{\tanh(\hbar\omega/2kT)}{(a\hbar\omega)^2}\right] \quad (4.3.1.4.2)$$

where $\hbar\omega$ is the oscillator energy, E_{ab} is the energy difference between the ground and the excited states, and a is the coupling constant that takes into account the electron lattice interaction.

In an intermediate crystal field, the excited electronic manifold $^4T_{2g}$ is shifted relative to the ground state $^4A_{2g}$ (Figure 4.3.1.2.1), and the transition energy (E_{ab}) for the transition $^4T_{2g} \longrightarrow {}^4A_{2g}$ becomes,

$$E'_{ab} = E_{ab} + \hbar\omega . n(\omega) - \frac{a^2}{2}\hbar\omega \quad (4.3.1.4.2)$$

where $n(\omega)$ is the distribution of vibrational states.

An example of the linear mode line shapes for the $^4T_{2g} \longrightarrow {}^4A_{2g}$ transition at temperatures T = 77, and 300 K, was plotted using Equation 4.3.1.4.2 and is shown in Figure 4.3.1.4.3a,b. The energy of the emission band at T = 77 K is clearly red shifted relative to the emission band at T = 300 K (Figure 4.3.1.4.3a).

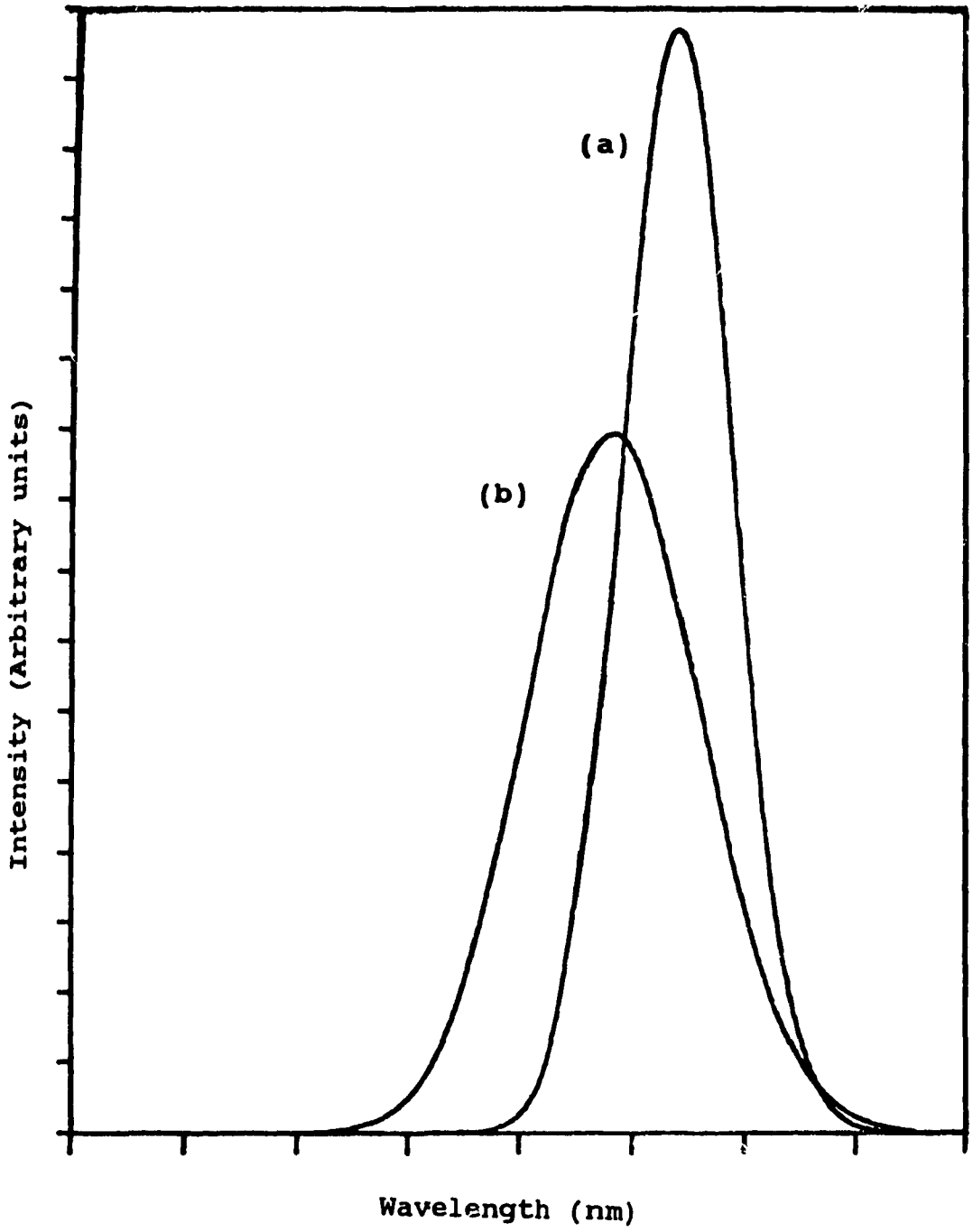

Figure 4.3.1.4.3 The line shapes due to the semiclassical approximation for the $^4T_{2g} \longrightarrow {}^4A_{2g}$ transition at (a) T = 77K ,and (b) T = 300 K.

We are now in a position to explain the shift towards lower energy of the $^4T_{2g} \longrightarrow {}^4A_{2g}$ transition At 77 K (Figure 4.3.1.4.1b). A schematic representation of the ground state $^4A_{2g}$ and excited state $^4T_{2g}$ energy levels in an intermediate crystal field are shown in Figure 4.3.1.4.4a,b. At a temperature T > 77 K, higher vibrational levels are occupied due to thermal equilibrium resulting in a $^4T_{2g} \longrightarrow {}^4A_{2g}$ transition which is higher in energy than the same transition at T > 77K (i.e) [E ($^4T_{2g} \longrightarrow {}^4A_{2g}$), T > 77K > E ($^4T_{2g} \longrightarrow {}^4A_{2g}$), T = 77K, Figure 4.3.1.4.4a,b].

Figure 4.3.1.5 a,b shows the resulting line shapes for the $^2E_g \longrightarrow {}^4A_{2g}$ transition at T = 77 and 300 k. The features that are immediately apparent are i) narrowing of the band shape at T = 77 k and ii) the line shapes are not shifted relative to one another (Figure 4.3.1.5 ab). This points to the fact that the $^2E_g \longrightarrow {}^4A_{2g}$ transition is totally independent of thermalization. Figure 4.3.1.4.4a,b schematically illustrates this point by showing that the energy of the $^2E_g \longrightarrow {}^4A_{2g}$ transiton is nearly the same at both low and high temperatures.

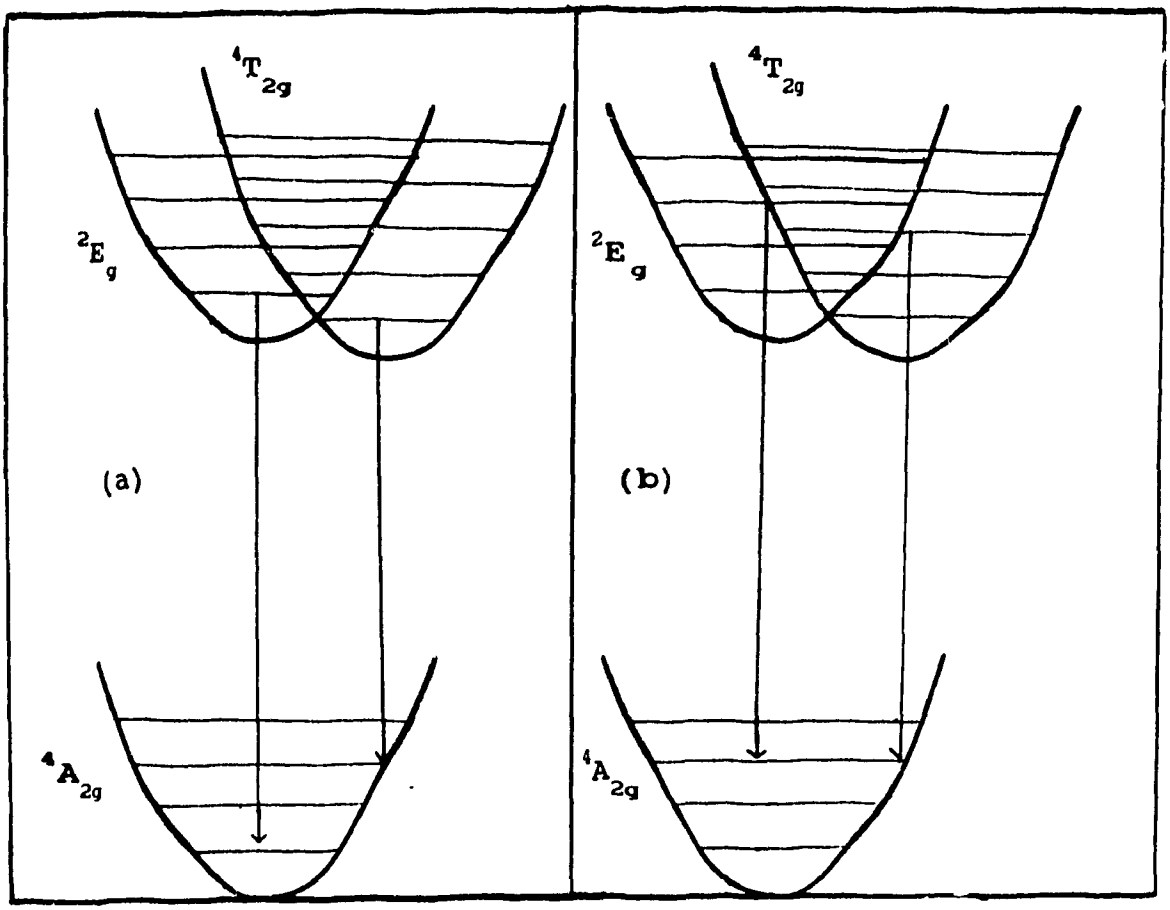

Figure 4.3.1.4.4 The simplified Tanabe-Sugano diagram showing the configuration coordinate diagram of Cr^{3+} energy levels and the possible transitions at (a) T = 77 K and (b) T > 77K.

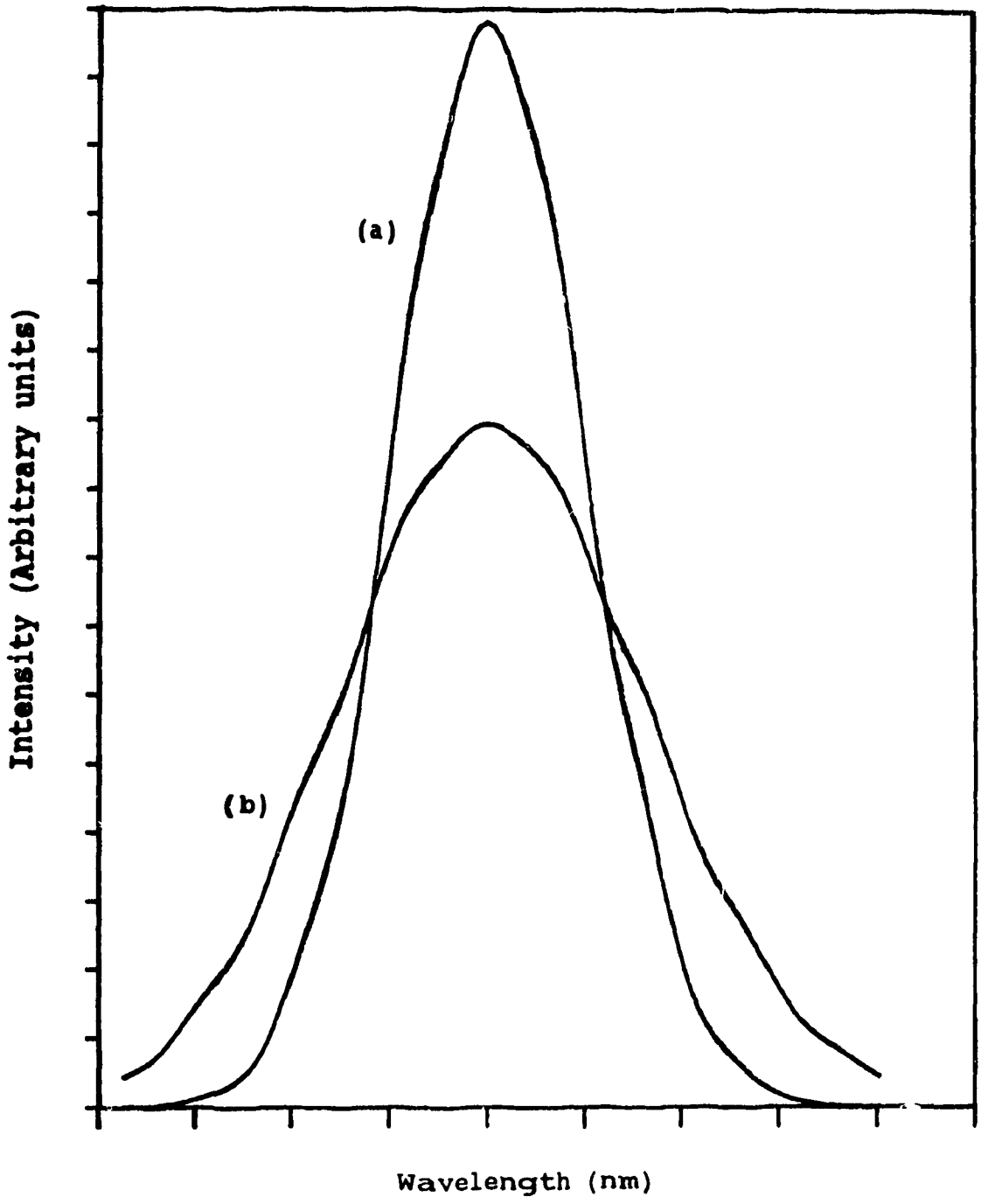

Figure 4.3.1.4.5 The line shapes due to the semiclassical approximation for the $^2E_g \longrightarrow {}^4A_{2g}$ transition at (a) T = 77K, and (b) T = 300 K .

4.3.1.5 TIME RESOLVED EMISSION IN CORDIERITE GLASS

Time resolved spectroscopy is invaluable since it enables an accurate distinction between the ^2E_g and $^4T_{2g}$ energy levels of Cr^{3+} and of the equilibrium between the population of the two levels.

The time resolved emission spectra at 77K of cordierite glass (NRC-3) excited at 573.95 nm are shown in Figure 4.3.1.5.1. The gatewidth was set at 150 μs and the delays varied from 0 μs to 150 μs. Figure 4.3.1.5.1 shows that for a delay of 150 μs the broad band centered at 840 nm disappears completely, while the narrower band centered at 692 nm persists. This confirms the band assignment of $^4T_{2g} \longrightarrow {}^4A_{2g}$ transition to the broader band at 840 nm and it is also in accordance with the spin selection rule $\Delta S = 0$. Since the $^2E_g \longrightarrow {}^4A_{2g}$ is spin forbidden, the probability of emission from that state is lower and therefore possesses a longer lifetime as shown in Figure (4.3.1.5.1).

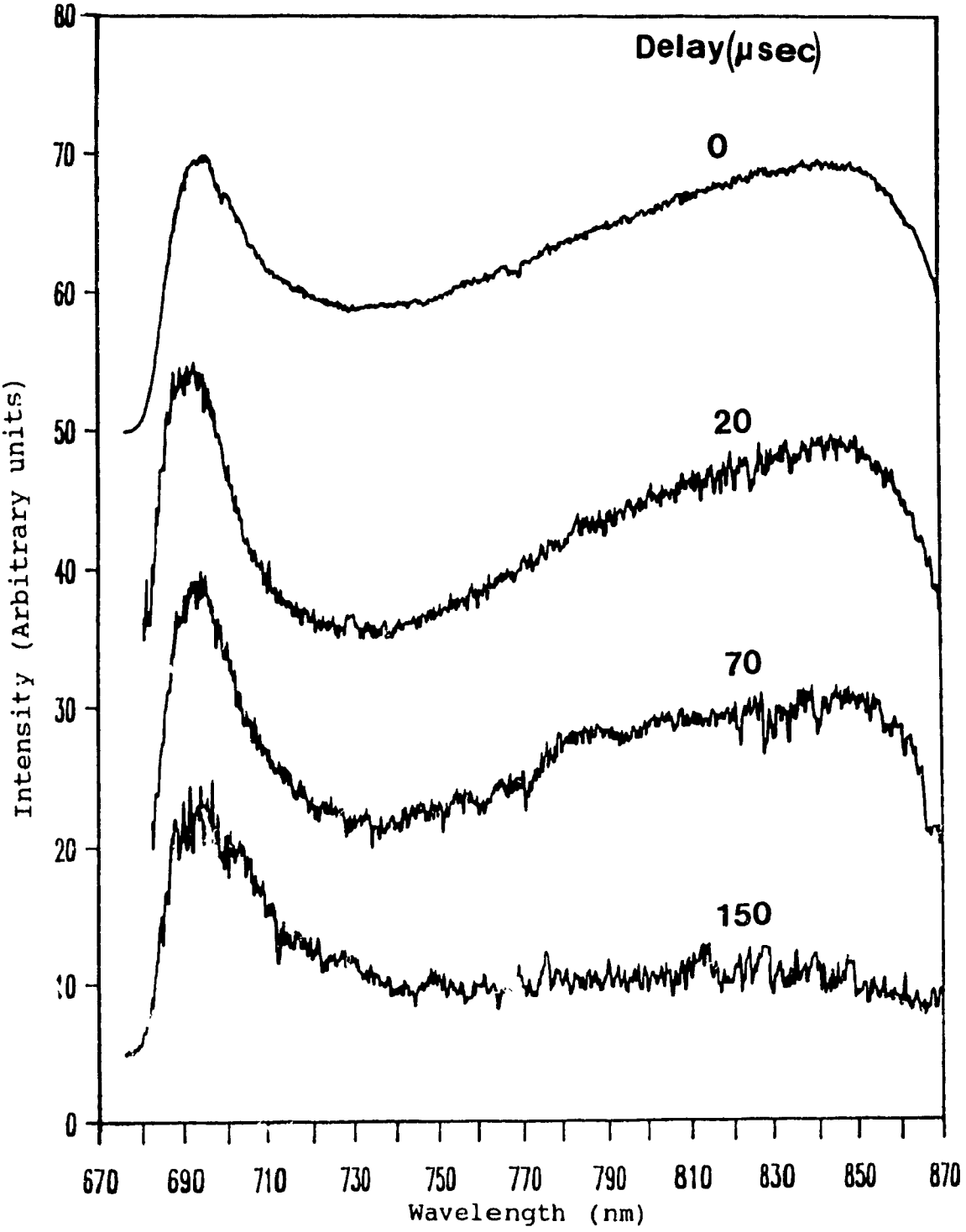

Figure 4.3.1.5.1 Time resolved emission spectra at 77K for cordierite glass (NRC-3), under 573.5 nm laser excitation at different delays. The gate width was set at 150 us.

4.3.1.6 DECAY MEASUREMENTS IN THE CORDIERITE GLASS

The $^2E_g \longrightarrow {}^4A_{2g}$ and $^4T_{2g} \longrightarrow {}^4A_{2g}$ transitions at 693 and 820 nm in the cordierite mother glass (NRC-3) have been found to decay approximately with 1.3 ms and 51.9 μs respectively at room temperature. These values are consistent for chromium (III) in glass [57]. Furthermore, it has been established that the glass possesses an intermediate field strength (Dq/B = 2.3).

Theoretically, if a system possesses an intermediate crystal field environment the energy separation between the $^4T_{2g}$ and ^2E_g energy levels should be nearly zero. This implies that it would be impossible from the decay measurements to recognize the ^4T and the ^2E_g levels because of the strong vibronic coupling of the excited energy levels assuming that the non radiative $^2E_g \longrightarrow {}^4T_{2g}$ transitions are rapid (Equation 4.3.1.4.1). The above arguement is in contradiction with the fact that the decay times are distinguishable.

This apparent contradiction may be resolved if we assume the co-existence of low, intermediate, and high field sites.

Wojtowicz and Lempicki [58] showed with mullite that although thermal equilibrium is achieved between the $^4T_{2g}$ and the ^2E_g energy levels for particular sites different sites will contribute luminescence with different quartet and doublet emission and with different decay times. Thus since the radiative lifetime $\tau(^2E_g)$ and $\tau(^4T_{2g})$ are vastly different, the effective lifetime will depend strongly on the spacing of these two levels. A crystal field varying from site to site (as is the case in glasses) changes the spacing and the order of the two excited states ($^4T_{2g}$ and ^2E_g) and a distribution of effective lifetime due purely to the crystal field variation will be obtained.

4.4 STRUCTURAL AND SPECTRAL CHANGES UPON MODIFYING THE MAGNESIUM OXIDE CONTENT IN THE MAGNESIUM ALUMINO-SILICATE SYSTEM.

A series of chromium doped magnesium alumino-silicate glasses (NRC-1 to NRC-7) were prepared by changing the MgO concentration to give $XMgO.Al_2O_3.2.5SiO_2$, where X varies from 0.50 to 2.0 (Table 3.1.1). It was found that a controlled change in the modifier content (MgO) for this particular oxide glass produced a "transparent" glass ceramic of high optical quality without recourse to thermal treatments.

4.4.1 ABSORPTION IN THE CORDIERITE SERIES

Figure 4.4.1.1 shows the liquid helium absorption spectra of the "glass" with varying concentration of magnesium oxide. We note changes in the peaks positions and the appearence of another band at approximately 500 nm. This band is assigned to the $^2T_{2g} \longleftarrow {}^4A_{2g}$ transition. A particularly noticeable feature is that the $^4T_{1g}$, $^4T_{2g} \longleftarrow {}^4A_{2g}$ transitions are blue shifted with increasing MgO concentration which amounts to an increase in the Dq value.

4.4.2 CALCULATION OF THE CRYSTAL FIELD PARAMETERS IN THE CORDIERITE SERIES

The absorption data were used to calculate the crystal field parameters using the Tanabe Sugano matrices [37]. Dq and B were determined from the $^4T_{2g}$ and $^4T_{1g}$ transition energies. The resulting energies and the crystal field parameters are shown in Table 4.4.2.1. The estimated crystal field parameters point to small changes in the field strength of the activator ion between individual samples. The estimated values reflect the magnitude in the blue shift observed in the absorption spectra of the serie (Figure 4.4.1.1).

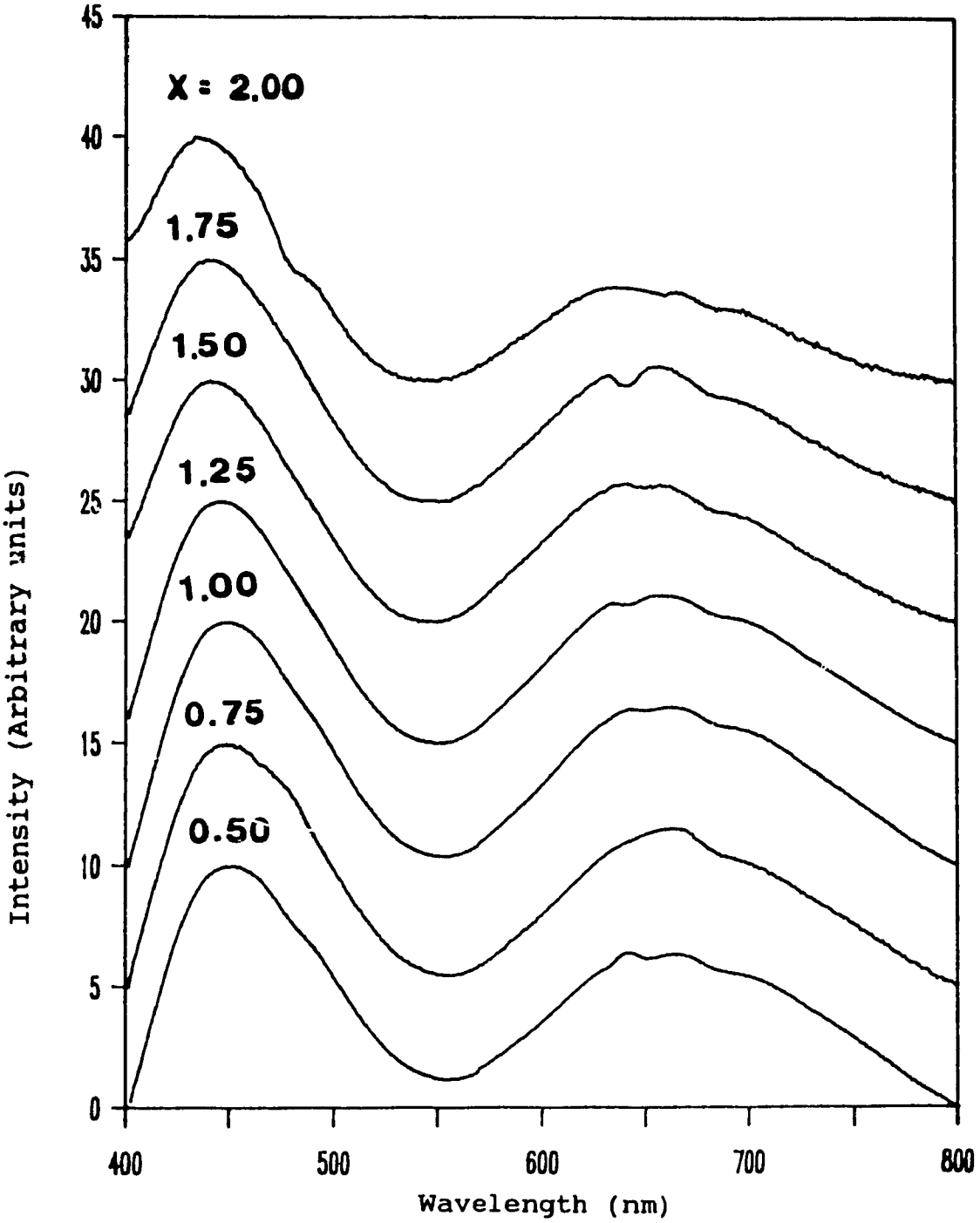

Figure 4.4.1.1 Liquid helium absorption spectra of Cr^3 in samples with varying MgO ($XMgO.2Al_2O_3.2.5SiO_2$) X = 0.5-2.0.

TABLE 4.4.2.1

SUMMARY OF SPECTROSCOPIC DATA FOR CHROMIUM (III) ABSORPTION IN $XMgO.Al_2O_3.2.5SiO_2$ WHERE X = 0.50-2.0. BAND POSITIONS IN UNITS OF WAVENUMBERS.

SAMPLE	$^2E_g \longleftarrow {}^4A_{2g}$	$^2T_{1g}$	$^4T_{2g}$	$^4T_{1g}$	D_q	B	C/B
NRC-1	14269	15262	15080	22168	1508	759	3.98
NRC-2	14301	15312	15130	22275	1513	767	3.93
NRC-3	14275	15259	15180	22279	1518	758	3.99
NRC-4	14255	15318	15150	22417	1515	787	3.77
NRC-5	14308	15290	15410	22576	1541	763	3.96
NRC-6	14292	15319	15410	22680	1541	780	3.83
NRC-7	14272	15378	15430	22881	1543	810	3.68

Figure 4.4.2.1 shows a plot of the oscillator strengths for the transitions $^4T_{2g}$, $^4T_{1g} \longleftarrow {}^4A_{2g}$ versus MgO concentration. We clearly see that the maximum oscillator strength of 1.81 X 10^{-4} ($^4T_{2g} \longleftarrow {}^4A_{2g}$) and 3.37 X 10^{-4} ($^4T_{1g} \longleftarrow {}^4A_{2g}$) occur for the mother glass (NRC-3), and are comparable to values obtained for other glass systems [59]. The fact that the maximum oscillator strength occurs for the mother glass is not surprising since in the glassy state Cr^{3+} resides in a lower symmetry than in the crystalline state thus lifting the parity forbidden d-d transitions.

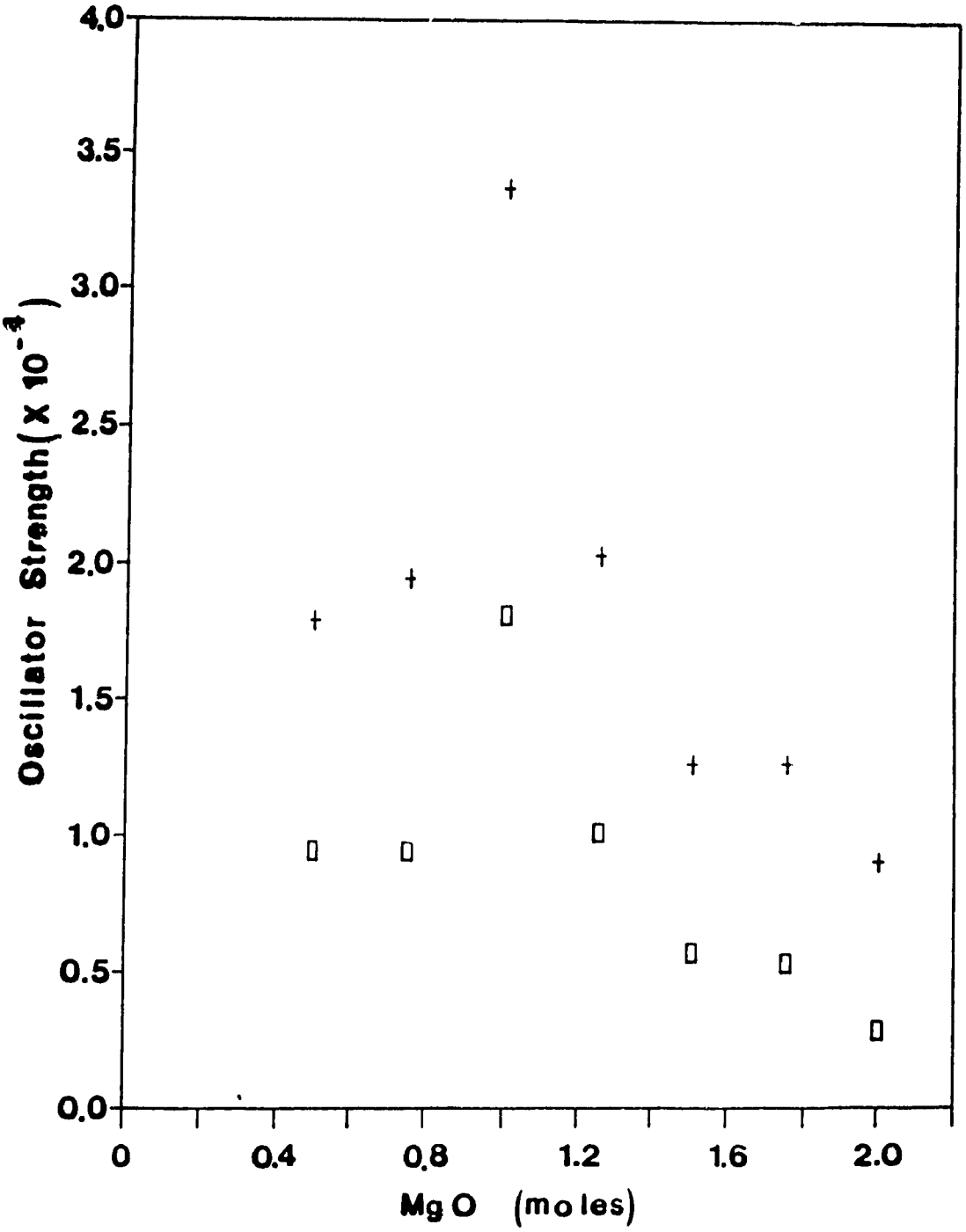

Figure 4.4.2.1 Behaviour of the oscillator strengths for the transitions $^4T_{1g} \longleftarrow {}^4A_{2g}$ (+) and $^4T_{2g} \longleftarrow {}^4A_{2g}$ (□) with varying MgO ($XMgO.Al_2O_3.2.5SiO_2$ X = 0.5-2.0).

The ocillator strength in glass ceramics for the transition $^4T_{2g} \longleftarrow {}^4A_{2g}$ containing gahnite has been found to be 0.52 X 10^{-4} [60], which is comparable to the values found in this study for the samples where crystallization is believed to be occuring.

4.4.3 EMISSION IN THE CORDIERITE SERIES

The emission spectra for Cr^{3+} in the mother glass and six samples of varying concentration at liquid helium temperature are shown in Figure 4.4.3.1. All of the spectra with the exception of NRC-1, NRC-2, and NRC-7 show two features: a broad band centered near 840 nm and a sharper feature near 694 nm. The broad band is assigned to the $^4T_{2g} \longrightarrow {}^4A_{2g}$ flourescence whereas the sharp feature is $^2E_g \longrightarrow {}^4A_{2g}$ R-line phosphorescence. The presence of the two bands indicates that both intermediate and low crystal field sites are present. The inhomogeneously broadened ^2E_g results from the wide range of crystal field sites.

The emission spectra of NRC-1, NRC-2 and NRC-7 show mainly sharp peaks and the broadband emission. Therefore the question which arises is if it is possible to identify the phase(s) within the sample that give rise to the sharp peaks and the broadband. We begin by examining the equilibrium diagram for the ternary system $MgO-Al_2O_3-SiO_2$ shown in Figure 4.4.3.2 [61].

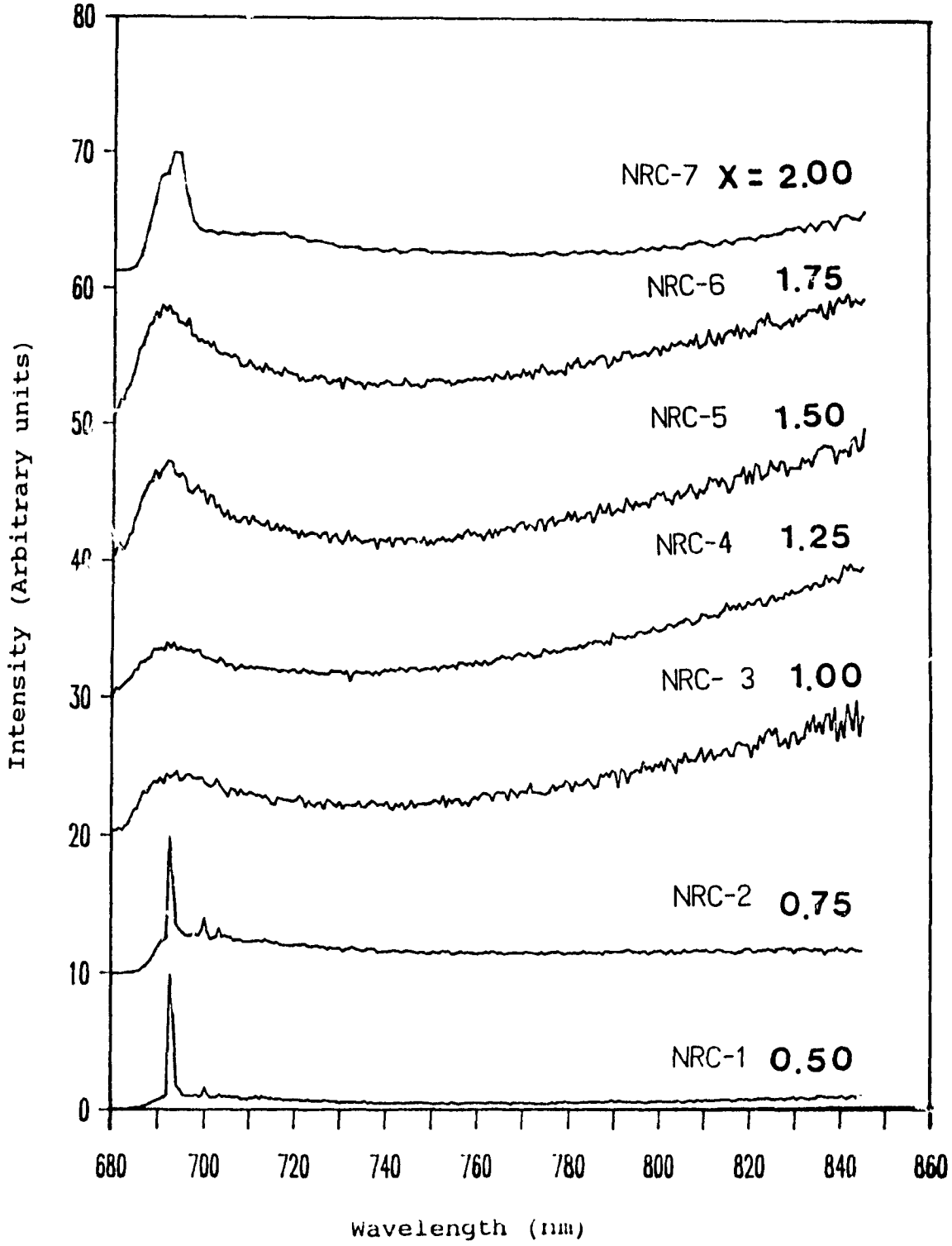

Figure 4.4.3.1 Liquid helium emission spectra of Cr^{3+} in samples with varying Mgo ($XMgO.2Al_2O_3.-2.5SiO_2$ X = 0.5-2.0)

This figure shows the presence of cordierite ($2MgO.2Al_2O_3.-5SiO_2$), sapphrine ($4MgO.5Al_2O_3.2SiO_2$), mullite ($3Al_2O_3.-2SiO_2$), forsterite ($MgO.SiO_2$), spinel ($MgO.Al_2O_3$), protenstatite ($MgO.SiO_2$), cristabolite (SiO_2), periclase (MgO) and corrundum (Al_2O_3).

Based on the equilibrium diagram the samples NRC-1 and NRC-2 are of composition which places them in the mullite region, whereas the samples NRC-3-4-5-6 and 7 in the cordierite region. The emission spectra of samples NRC-1 and NRC-2 is very similar to ruby ($Al_2O_3:Cr^{3+}$) [62]. Therefore the peak at 693 nm (Figure 4.3.7.2.4) can be assigned to the zero phonon $^2E_g \longrightarrow {}^4A_{2g}$ line (R_1) and the two peaks at approximately 700 and 704 nm to the N_2 and N_1 lines respectively [16]. Further evidence was provided from the lifetime of the R_1 line (3 ms) which is very similar to what is found for $Al_2O_3:Cr^{3+}$ [63].

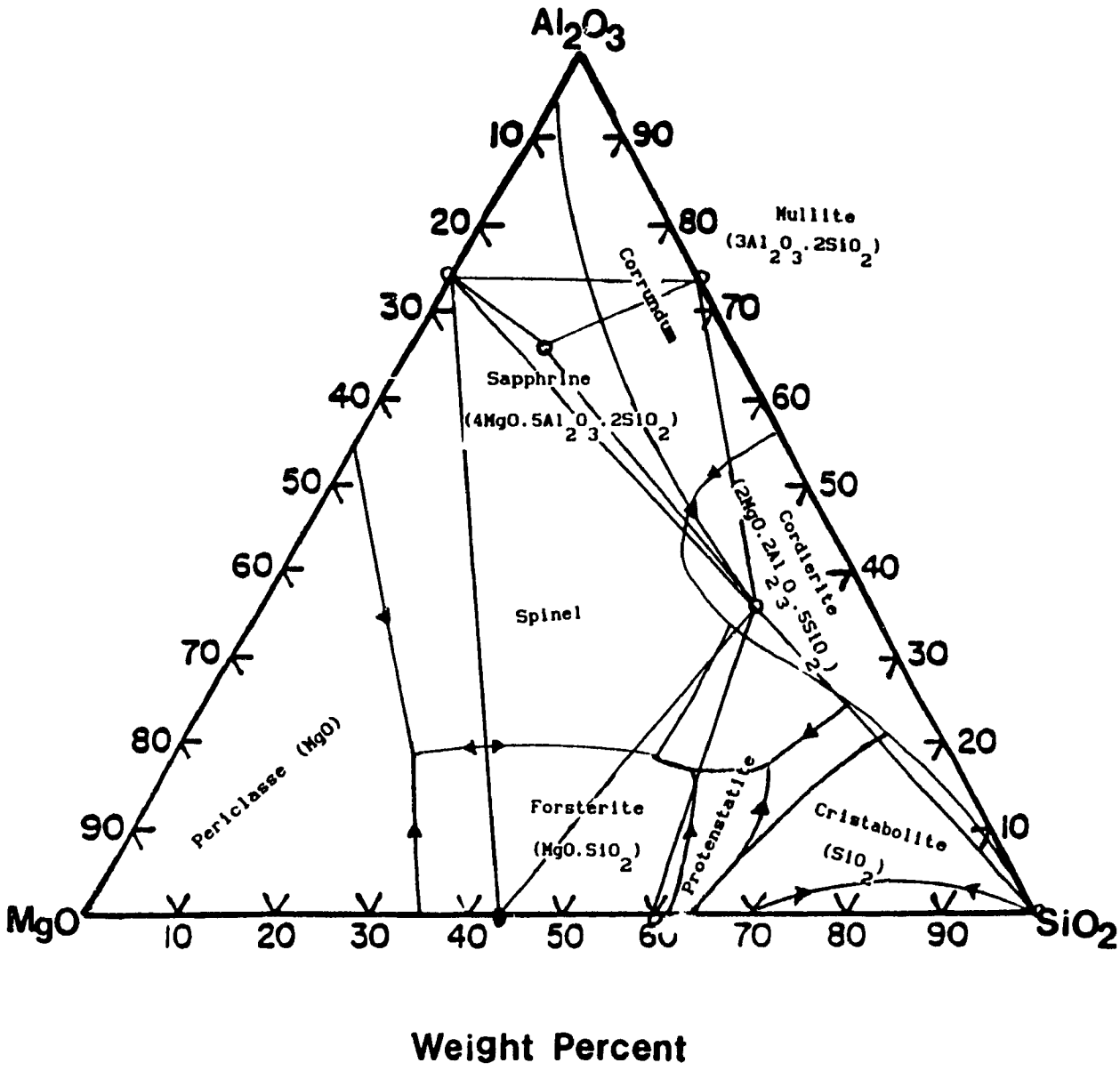

Figure 4.4.3.2 Equilibrium diagram of the system $MgO-Al_2O_3-SiO_2$.

The emission spectra of samples NRC-1 and NRC-2 at room temperature (Figure 4.4.3.3) show conclusive evidence of the $Al_2O_3:Cr^{3+}$ crystalline phase. The spectrum is characterized by two sharp peaks at 693 nm that are separated by 30 cm^{-1} ($Al_2O_3:Cr^{3+}$ splitting = 29 cm^{-1}) and are assigned to the R_1 and R_2 splitting of the ^2E_g state. The origin of the splitting is shown schematically in Figure 4.4.3.4 [64].

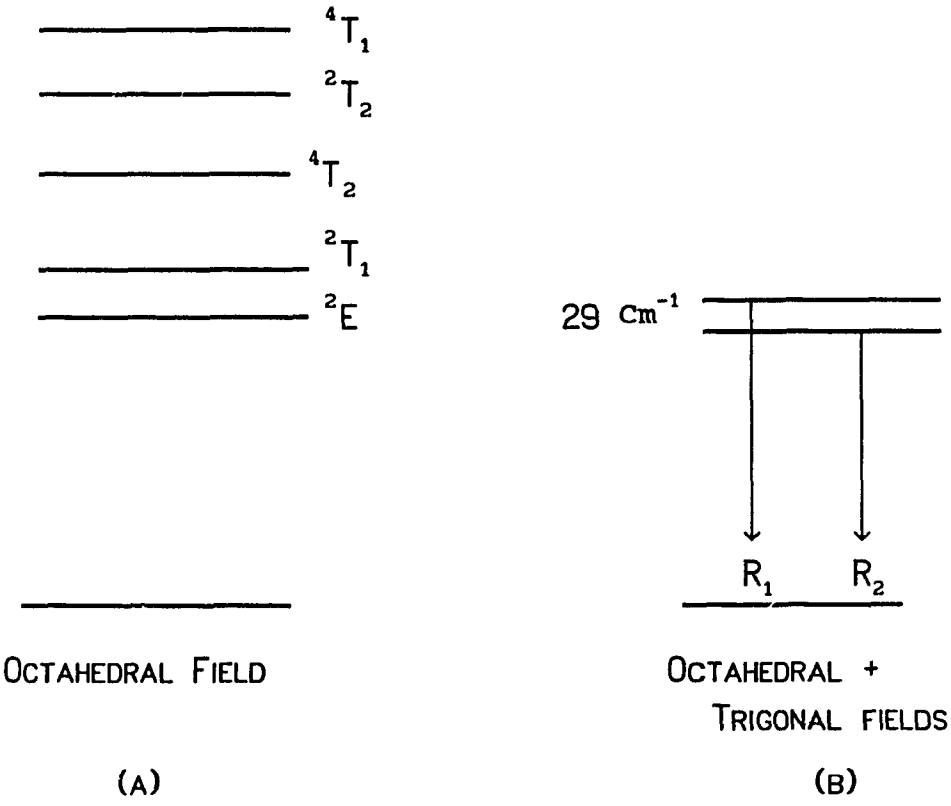

Figure 4.4.3.4 Energy level diagram of Cr^{3+} in an octahedral field (a) Fine structure in the ^2E level. The 29 cm^{-1} splitting in the ^2E states results in two sharp fluorescence lines found in $Al_2O_3:Cr^{3+}$ (b).

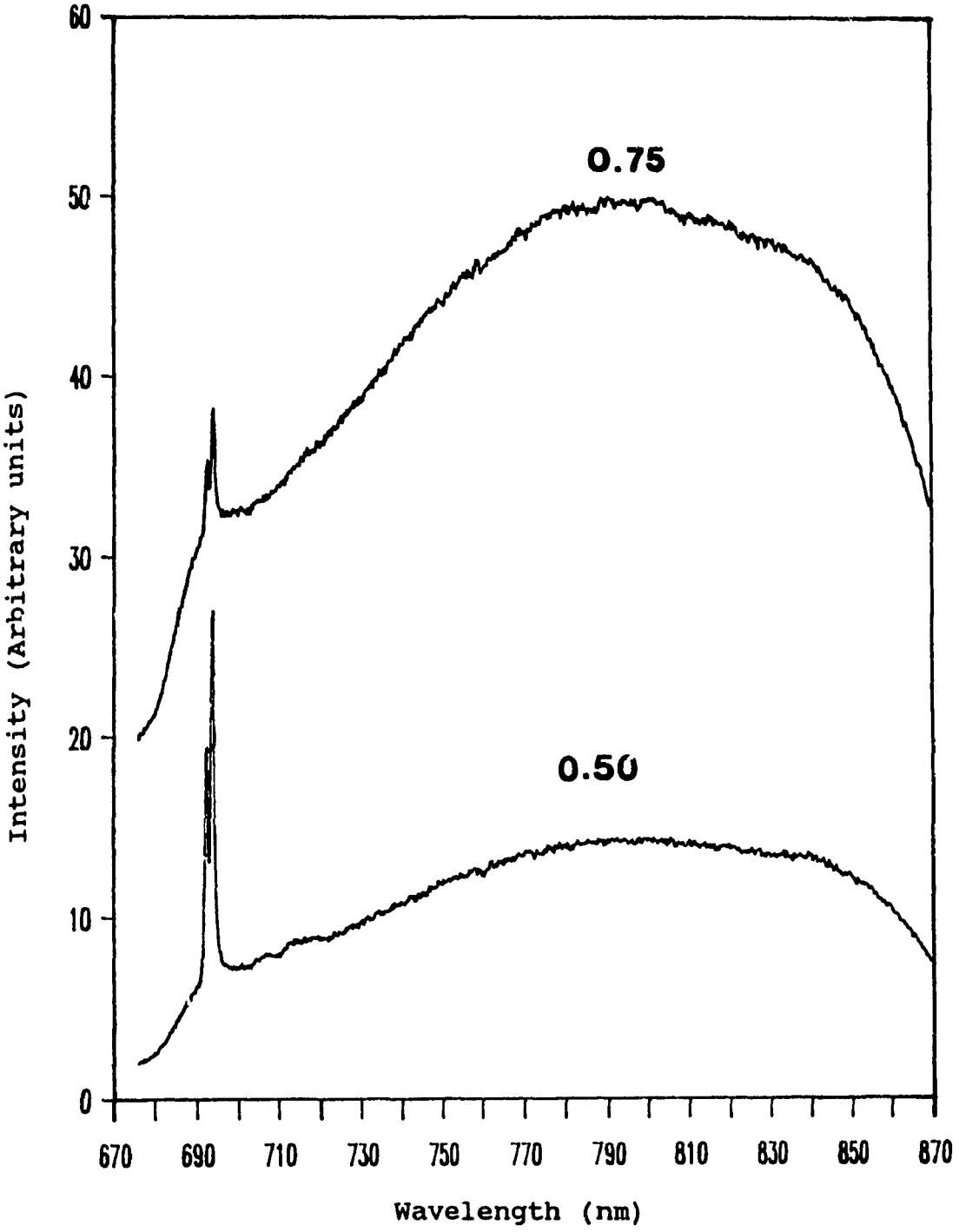

Figure 4.4.3.3 Room temperature emission spectra of Cr^{3+} in samples with varying MgO ($XMgO.2Al_2O_3.-2.5SiO_2$ X = 0.5, 0.75)

It is worth noting that at 10 K, the emission spectra of the samples NRC-1 and NRC-2 (Figure 4.4.3.1) do not show the splitting pattern (R_1 and R_2 lines) of the ^2E_g energy level. This is a simple consequence of the Boltzmann distribution which is conveniently written as,

$$\frac{N_{Upper}}{N_{Lower}} = \exp(-\Delta E/kT) \qquad 4.4.3.1$$

where N_{Upper} / N_{Lower} is the ratio of the population of electrons between an upper and lower vibrational level, ΔE refers to the spacing between the vibrational levels. At 10 K the ratio N_{Upper} / N_{Lower} is negligible. Thus, the spectra of the samples NRC-1 and NRC-2, show transtions originating only from the R_1 line of the ^2E_g energy level.

This conclusion is not unreasonable if we consider; (i) the composition of the samples NRC-1 and NRC-2 places them in the mullite region and (ii) the MgO concentration is not high enough for the formation of stoichiometric cordierite. Therefore, the situation arises where both the formation of mullite glass, and the crystallization of Al_2O_3 is occuring. The Cr^{3+} ions partition between the mullite glass phase which gives rise to the residual broadband in the emission spectra and MgO which results in the sharp peaks.

Upon increasing the MgO content from X = 1.00 to 1.75 it was observed that the emission spectra are typical of glass.

The composition of these samples (NRC-3-4-5 and 6) is such that it places them in the cordierite region of the equilibrium diagram, therefore, the emission and absorption spectra are typical of Cr^{3+} in cordierite glass [63].

The equilibrium diagram (Figure 4.4.3.2) predicts the formation of cordierite and the magnesium spinel ($MgAl_2O_4$) for the sample NRC-7. The emission spectrum of this sample (Figure 4.4.3.3) is composed of a prominant $^2E_g \longrightarrow {}^4A_{2g}$ emission and broadband $^4T_{2g} \longrightarrow {}^4A_{2g}$ transition. The $^2E_g \longrightarrow {}^4A_{2g}$ transition shows two broad lines at 690.3 nm and 692.2 nm which can be assigned to two types of Cr^{3+} ion in $MgAl_2O_4$ which has undergone inversion [65-67], whereas the broadband is typical of glasses and is assigned to Cr^{3+} ions in cordierite glass [63].

Spectroscopically, it was found that the samples NRC1 and NRC-2 consists of microcrystallites of mullite, where the Cr^{3+} ions reside mainly in the alumina phase as (Cr^{3+}:Al_2O_3). On the other hand, the samples NRC 3, 4, 5, and 6 have shown no evidence of phase separation, and were identified as the cordierite glass ($MgO.Al_2O_3.2.5SiO_2$) based on the phase diagram. Finally, the sample NRC-7 was identified spectroscopically, and found to contain the Mg spinel phase ($MgAl_2O_4$) as the crystalline phase. These changes can be explained in the following manner.

From a structural point of view, magnesium is a modifier. These cations occupy holes or intersitial sites thus "modifying" the continuous random network of a glass by breaking it up.

In other words, the modifier opens the glass structure by breaking bonds producing the so called "dangling bonds or "non-bridging" oxygens; this process is shown schematically in Figure 4.4.3.5.

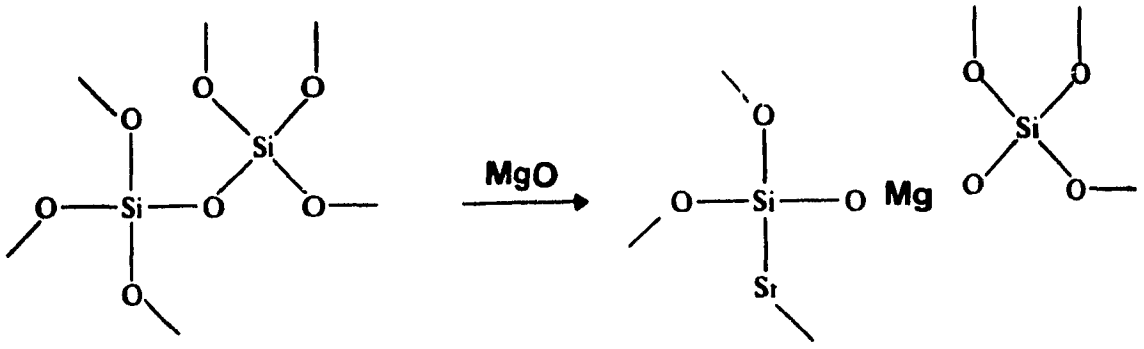

Figure 4.4.3.5 Schematic illustration of the effect of the addition of the alkali oxide MgO to silica. Each molecule added converts a bridging oxygen to two non-bridging oxygens.

The reason that bonds break in the presence of Mg^{2+} is that a repulsive potential is build up between the cation that makes up the glass network, Si^{4+}, and to a lesser extent Al^{3+}, and the modifier, Mg^{2+} ion,.

The effect of Mg^{2+} therefore is such as to maintain a minimum "internal energy", (by expanding the polyhedra within the network), necessary to keep the glassy matrix aperiodic.

The other component that plays an important role is the Cr^{3+} ion. It must be remembered that Cr^{3+} not only acts as a probe ion, but is also a nucleating agent. At a certain critical concentration, it acts by raising the interfacial surface energy ,γ, thus lowering the energy ,ΔG_v, (Equation (4.4.3.1)) [33] necessary to form a new crystalline phase.

$$\Delta G = \frac{4}{3}\pi r^3 \Delta G_v + 4\pi r^2 \gamma \qquad (4.4.3.1)$$

ΔG_v is the change in the free energy per unit volume associated with a phase transformation of the supercooled liquid to a solid crystalline phase, γ is the interfacial energy per unit area, and ΔG is the total energy. Mg^{2+} serves to maintain an amorphous network, however, Cr^{3+} raises the internal energy and promotes crystallization since an amorphous phase possessing an internal energy considerably higher than the crystal would lead to rapid devitrification: The ratio $\left[MgO\right]_{CONC.}$: $\left[Cr^{3+}\right]_{CONC.}$ determines whether the glass will remain amorphous or phase separates into regions of microcrocrystallites embedded in the glass.

Table 4.4.3.1 summarizes the results obtained spectroscopically, and the relation between the concentration of MgO, the number of non-bridging oxygen (NBO), and the type of network obtained.

TABLE 4.4.3.1

THE VARIATION OF THE AVAILABILITY OF NON-BRIDGING OXYGENS BY CHANGING THE CONCENTRATION OF MAGNESIUM OXIDE.

X MgO .Al_2O_3.2.5SiO_2 0.11% Cr^{3+}

SAMPLE	X	% MgO (MOLE)	NBO/Cr^{3+}	PHASES OBTAINED CRYSTALLINE	GLASS
NRC-1	0.5	3.70	70	(Al_2O_3:Cr^{3+}) /	MULLITE
NRC-2	0.75	9.10	175	(Al_2O_3:Cr^{3+}) /	MULLITE
NRC-3	1.0	16.66	340	———	CORDIERITE
NRC-4	1.25	25.20	556	———	CORDIERITE
NRC-5	1.50	26.70	640	———	CORDIERITE
NRC-6	1.75	31.60	710	———	CORDIERITE
NRC- 7	2.0	37.40	820	($MgAl_2O_4$: Cr^{3+}) /	CORDIERITE

NBO = NON-BRIDGING OXYGENS

As shown in Table 4.4.3.1, samples NRC 3-6 are cordierite glass. One observes that below 16.66 mole % MgO, (X = 0.5, 0.75 NRC1, NRC2) the formation of the glass ceramic with Al_2O_3 as the crystalline phase. The lower magnesium content reduces the number of dangling or non-bridging oxygens, thus the glass is energetically less favourable.

Furthermore, the ratio of magnesium to Cr^{3+} decreases in going from NRC 3 to NRC 1. Hence, the greater number of chromium ions per magnesium ions create regions rich in the nucleating agent. This promotes the rate of formation of the microcrystallites Al_2O_3 in the glass.The formation of the spinel (NRC-7, $MgAl_2O_4$) phase can be explained on the basis that once stoichiometric cordierite glass was formed upon cooling the melt (below the liquidus point), there remained sufficient magnesium that resulted in the formation of the spinel. This is not unreasonable since NRC-7 contains the highest magnesium content (37.4 % mol MgO) in the series.

4.5 HEAT INDUCED CERAMITIZATION OF CORDIERITE GLASS

A Cordierite glass doped with 0.17 % Cr_2O_3 was prepared using the same melting and annealing teperatures as for the cordierite series. It was later heat treated at 1100°C for 2 hours and crystallized at 1250°C for 4-5 hours to produce an opaque pink ceramic. The sample will be referred to as NRCC from this point onward. The purpose is to describe the spectroscopic properties of the ceramic and from there to be able to identify the crystalline phase present.

4.5.1 EXCITATION SPECTRUM OF THE CERAMITIZED CORDIERITE

In Figure 4.5.1.1 we show the excitation spectrum of the Cr^{3+} doped ceramic (NRCC) and the absorption spectrum of the cordierite glass (NRC-3).

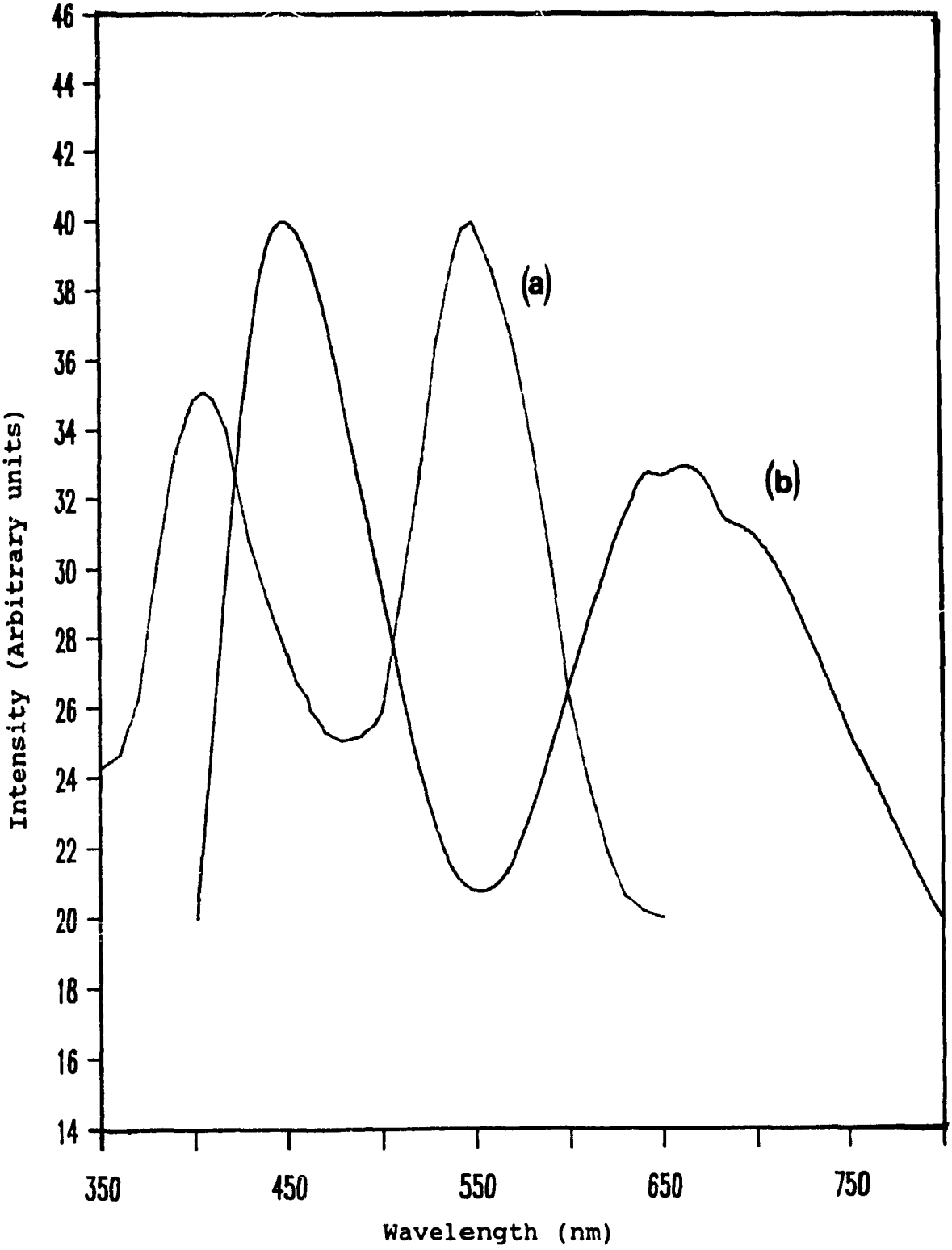

Figure 4.5.1.1 Excitation spectra of the ceramitized cordierite (NRCC)(a) compared to the absorption of spectrum of cordierite glass (NRC-3) (b). at liquid helium temperature.

When the glass is subjected to heat treatment to form the ceramic, the Cr^{3+} excitation spectrum undergoes a change in the positions of the quartet-quartet transitions ($^4T_{1g}$, $^4T_{2g} \longleftarrow {}^4A_{2g}$). The transitions are blue shifted to 400 nm and 550 nm respectively.

We calculated the value of Dq for both the cordierite glass and ceramic and found values of 1575 cm^{-1} and 1818 cm^{-1} respectively. This allows us to conclude that there has been an increase in the crystal field in going from the glass to the ceramic.

The halfwidths also provide information about the distribution of field strengths of the activator ion in the glass and the ceramic. For the Cordierite glass (NRC-3) the transition $^4T_{2g} \longleftarrow {}^4A_{2g}$ has a halfwidth of 2700 cm^{-1} compared to a halfwidth of 2000 cm^{-1} for the ceramic The decrease in bandwidth in going from the glass to the ceramic is attributed to ordering, which results in a more symmetrical environment in the crystalline phase. The question that arises is why the activator ion when given a choice, migrates from an amorphous environment into a crystalline phase of higher symmetry? This can be explained in terms of the ligand field stabilization energy which has a value of about 5 times greater in crystalline solids [47].

4.5.2 EMISSION IN THE CERAMITIZED CORDIERITE

Figure 4.5.2.1 shows the emission spectrum of the ceramic (NRCC) excited at 573.0 nm. The spectrum is characterized by the two intense emission bands centered at 688 and 692 nm that can be attributed to the $^2E_g \rightarrow {}^4A_{2g}$ transition. These two broad bands are known as N_3 lines and correspond closely to the N_3 lines in the emission spectrum of the chromium doped spinel ($Cr^{3+}:MgAl_2O_4$) reported by Mikenda and Preisinger [68].

The halfwidths of the peaks positioned at 688 and 692 nm have been estimated to be 63 and 65 cm^{-1} respectively (Figure 4.5.2.1). Based on this, the N_3 lines cannot be assigned to the R_1, R_2 splitting of the ^2E_g level. These values for the halfwiths are much greater than those reported for Cr^{3+} in crystalline solids such as ruby ($Al_2O_3:Cr^{3+}$, BWHM = 30 cm^{-1}).

The X-ray diffraction pattern of the ceramic shown in Figure 4.5.2.2 confirms that the only crystalline phase present is the magnesium spinel ($MgAl_2O_4:Cr^{3+}$). The ceramic sample was determined to be biphasic and consists of a crystalline phase embedded in a glassy phase. The residual glass is indicated by the broad band between 10 to 15° (θ).

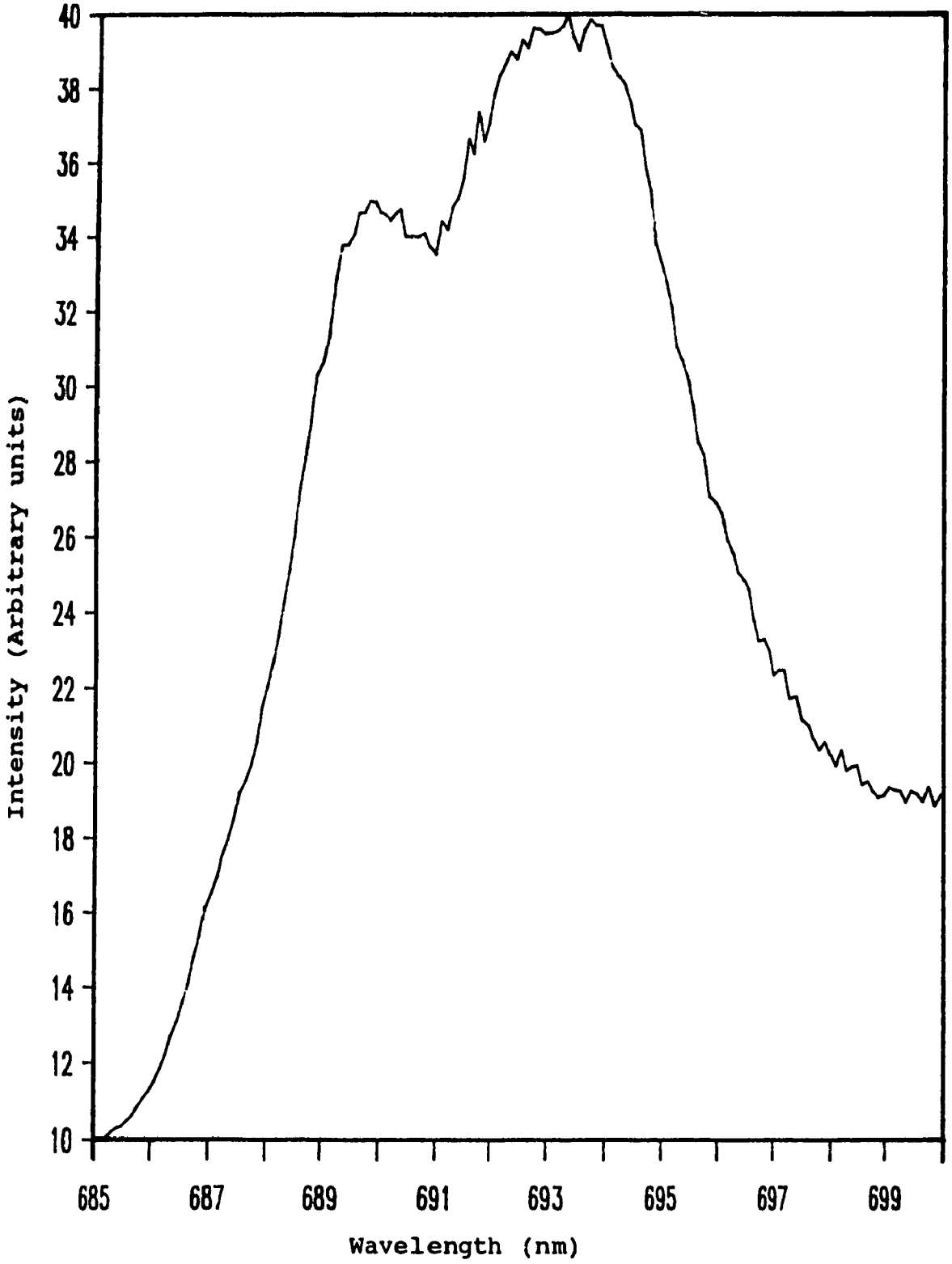

Figure 4.5.2.1 Emission spectrum taken at 77 K for the ceramitized cordierite ceramic (NRCC) excited 573.0nm

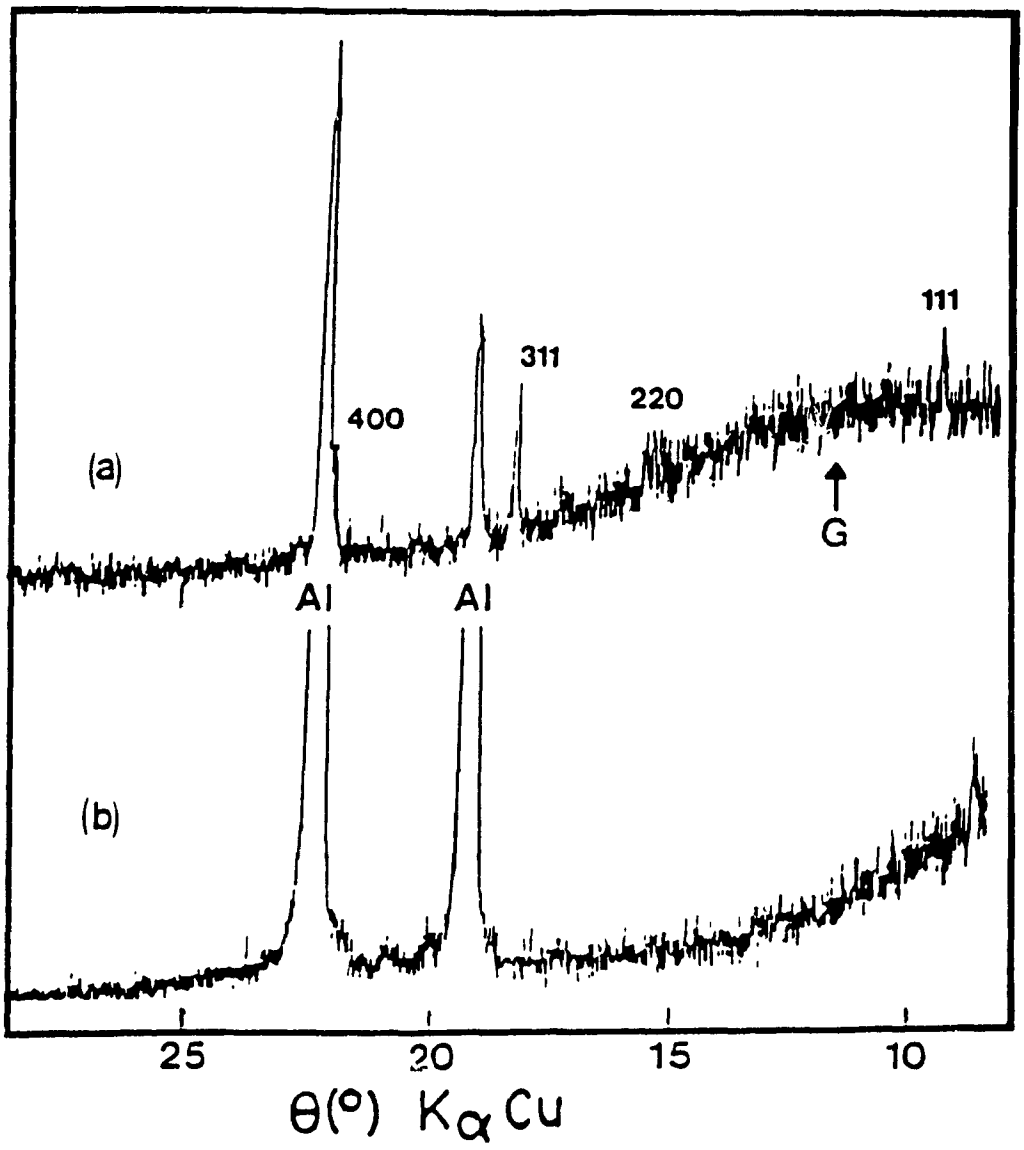

Figure 4.5.2.2 X.R.D. pattern for a completely ceramitized sample cordierite (NRCC) (a). X.R.D. pattern for the aluminum sample holder (b).

The question arises as to the specific nature of the luminescence centers which give rise to the emission of these lines. The N lines are structure dependent and are the result of pertubations, in the positions of the Cr^{3+} energy levels. One can account for the presence of the two bands with maxima at 688 and 686 nm by assuming that there are two classes of Cr^{3+} ions.

The first type or class of Cr^{3+} ions are those that occupy the normally ordered spinel, where the octahedral positions are completely occupied by Cr^{3+} ions. In Figure 4.5.2.3 a schematic representation of a direct or "normal spinel" ($A^{[tet]}B_2^{[oct]}O_4$) is shown [69]. It crystallizes in the $Fd3m\text{-}O_h$ (N0.227). The Mg^{2+} cations occupy tetrahedral position A (8a Wyckoff site) with a T_d site symmetry, whereas Al^{3+} cations occupy a trigonally distorted octahedral site, B sites, with a D_{3d} site symmetry.

The second class of Cr^{3+} ions result from the degree of inversion that is always present in synthetic spinel samples like our material [71]. The degree of inversion, (i = 10%-30%), for synthetic samples may be written as

$$i = \frac{Mg(6)}{Mg(6) + Mg(4)} \qquad (4.5.2.1)$$

where Mg(6) = Mg^{2+} in octahedral coordination, and Mg(4) = Mg^{2+} in a tetrahedral coordination.

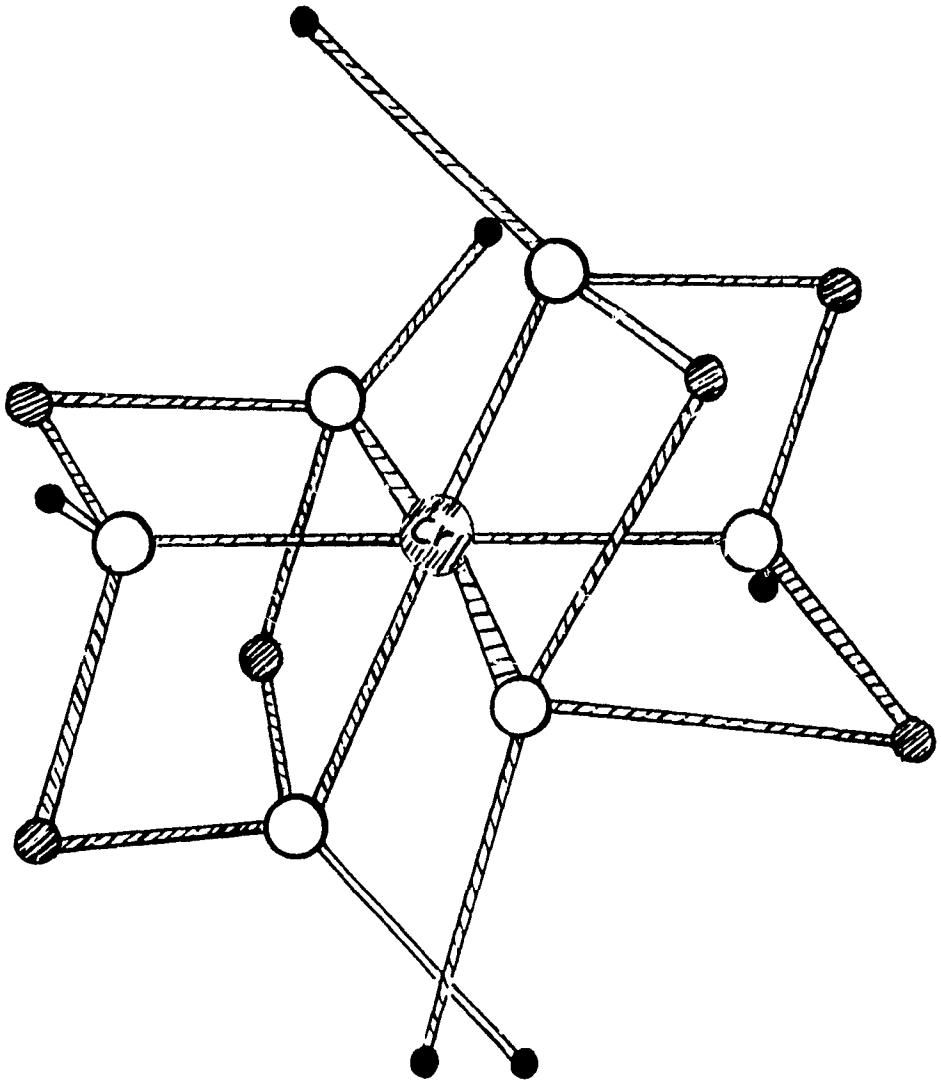

Figure 4.5.2.3 Stereoscopic view of octahedral Cr^{3+} in the spinel network

Due to the degree of inversion, the cation distribution within the first two coordination spheres of the substitutional Cr^{3+} ions deviate from the normal distribution resulting in the second class of Cr^{3+} ions. The inhomogeneity of the two broad lines at 688 nm (BWHM = 63 cm^{-1}) and 692 nm (BWHM = 65 cm^{-1}) can be associated with small site to site energy differences due to "second" nearest neighbors.

4.5.3 CHROMIUM PAIR INTERACTION IN THE CERAMITIZED CORDIERITE

Figure 4.5.3.1 shows the complete emission spectrum of the chromium doped ceramic (NRCC). The spectrum is characterized by two bands with maxima at 688 and 692 nm and two broader bands centered at 710 and 740 nm. Note that the origin of the bands at 688 and 692 nm was dealt with in the previous section.

The band at 710 nm is attributed to the presence of chromium pairs. This situation occurs when two Cr^{3+} ions are in nearby sites interacting antiferomagnetically and creating exchanged coupled pairs that have characteristic lines at 710 nm [70]. Significant exchange pairs of Cr^{3+} emission in crystals ordinarily appear when the concentration of the dopant is 0.3 mole % [70]. In the 0.17 % Cr_2O_3 ceramic sample (NRCC), the Cr^{3+} concentration is 0.08 mole %.

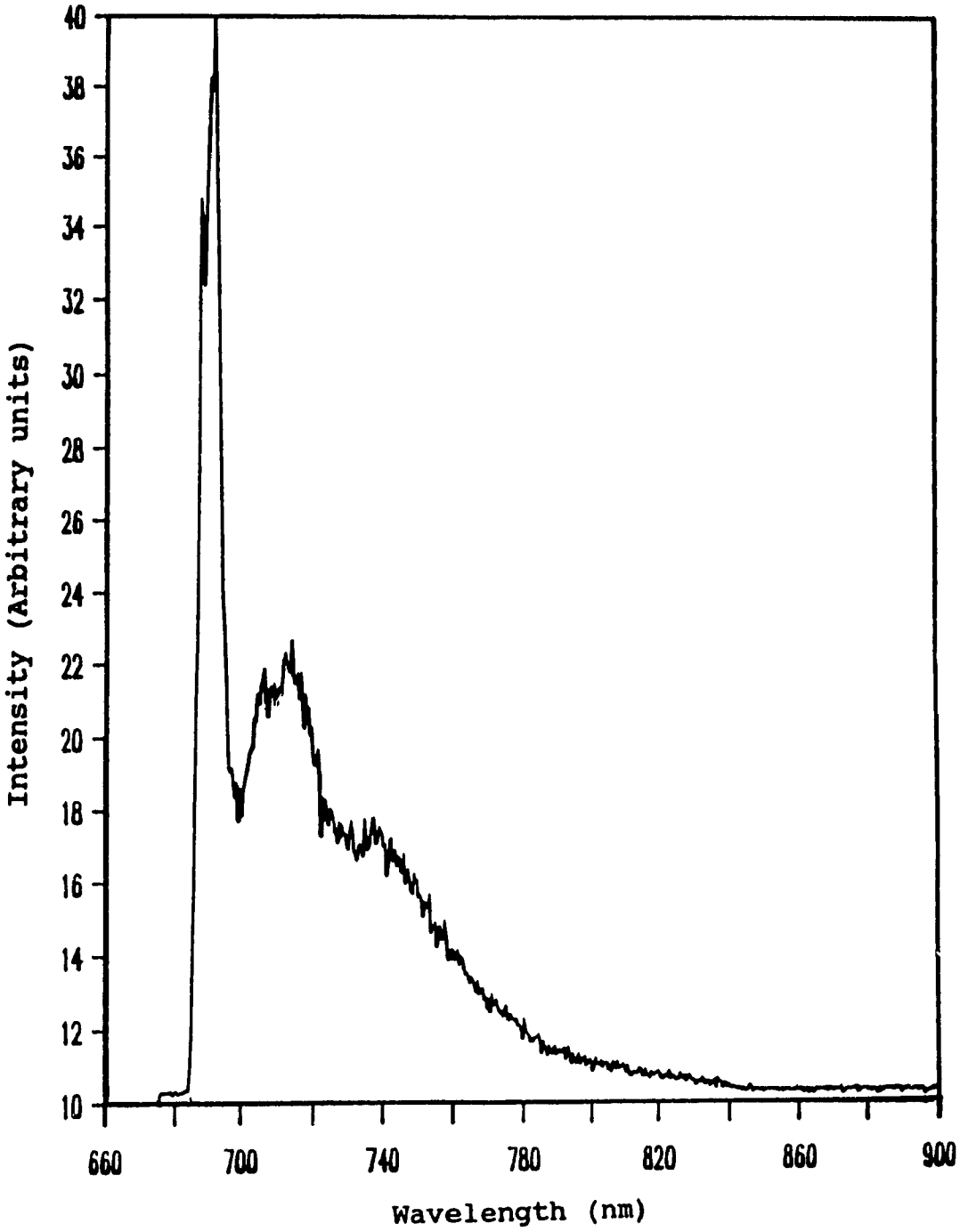

Figure 4.5.3.1 Emission spectrum of cordierite ceramic (NRCC) doped with (0.17 Cr_2O_3) excited at 573 nm at 77K.

Even at this concentration chromium pair interaction must be occuring to a considerable degree as evident from the appearence of the band at 710 nm. This may be due to the possibility that the Cr^{3+} ions are distributed unevenly between the crystalline and the residual glass phase (Figure 4.5.2.2). The question arises as to whether Cr^{3+} would partition equally between the two phases. Although it is energetically less favorable, the amorphous siliceous network contains large polyhedra able to accept Cr^{3+} as a network modifiers.

Therefore we can imagine that during the crystallization process of NRCC a significantly greater number of activator ions migrated into the crystalline phase. Clearly, this implies that the concentration of Cr^{3+} is greater in the Mg-spinel phase.

The broad emission band centered at 740 and extending to 840 nm (Figure 4.5.3.1) can be attributed to the transition $^4T_{2g} \longrightarrow {}^4A_{2g}$ and is due to Cr^{3+} ions in low crystal field sites. This is reasonable since some of the chromium ions have probably remained in the residual glass phase.

CHAPTER 5

CONCLUSION

In this thesis we have presented the luminescent properties of Cr^{3+} doped ($XMgO.Al_2O_3.2.5SiO_2$) in three distinct phases. These are the cordierite glass ($MgO.Al_2O_3.2.5SiO_2$, NRC3) , glass ceramic (X = 0.5 - 2.0, NRC 1 - 7), and finally the completely ceramitized cordierite produced by subjecting the precursor cordierite glass to a heat treatment schedule.

The cordierite series NRC 1 - 7, consist of cordierite glass and glass ceramics of high optical qualities that can be easily synthesized in the $XMgO.Al_2O_3.2.5SiO_2$ system without recourse to thermal treatments. The most significant results are :

(i) The changes in the emission spectra which are consistent with the formation of a glass ceramic (X = 0.50 and X = 0.75), glass (X = 1.0 - 1.50) and glass ceramic (X = 1.75 - 2.0).

(ii) Evidence that Cr^{3+} is found in both crystalline and glass phase of the glass ceramic.

(iii) The crystalline phases have been identified as aluminum oxide (Al_2O_3), and magnesium spinel ($MgAl_2O_4$), and the glass phases mullite ($3Al_2O_3.-2SiO_2$) and cordierite ($MgO.Al_2O_3.2.5SiO_2$).

These conclusions raise a number of questions:

1) What are the sizes of the crystallites found in the glass ceramic present in the cordierite series?

Raman spectroscopy can be used to determine crystallite size, since the size of the crystallites is directly related to the position of their surface vibration modes [71].

Glass ceramics are of interest for laser technology because they combine the advantage of crystalline hosts (quantum yield close to unity) with relative ease of the manufacturing tecnology of glasses. The size of crystallites is a factor that determines the possibility of a host material to lase. However, as Wojtowicz and Lempicki aptly stated:

> *"Laser application will be ultimately determined by the possibilty to reduce scattering losses by at least an order of magnitude. Should that prove possible the technology of ceramics will make them stronger contenders for large scale lasers" [72].*

The next question is whether any of the materials produced show a gain?

This can be answered by employing a technique called pump probe. In this technique, a laser is used as the pump source, to induce stimulated emission in the sample, and a second laser, the probe, is employed to determine whether the emission from the sample shows a gain.

CHAPTER 6

REFERENCES

1) S.E. Stokowski., in Lasers, Spectroscopy and New Ideas (eds W.M. Yen and M.D. Levenson), vol 54. Springer Verlag P. 47 (1987).

2) W.H. Zachariasen, J. Am. Chem. Soc., 54, 3841 (1932).

3) W.B. White, D.S. Knight, Reprinted from Defects in Glass F.L Galeener, D.L. Griscom, and M.J. Weber, (eds. Proc. Materials Res. Soc. 61, 283, (1986).

4) K.H. Sun, J. Am. Cer. Soc., 30, 9, 277, (1947).

5) G.W. Morey The Proprerties of Glass Reinhold Publishing Corporation P.16, (1938).

6) T. Bates, in Modern Aspects of the Vitreous State, (ed. J.D. Makenzie Butterworths, London) P.195. (1962)

7) J. Wong, C.A. Angel, Glass Structure By Spectroscopy, (Marcel Dekker, New York) (1976).

8) S.T. Lai and M.L. Shand. High efficiency CW laser-pumped tunable alexandrite laser. J. Appl. Phys., 54, 5642 (1983).

9) J.C. Walling, O.G. Peterson. H.P. Jenssen, R.C. Moris, and E.W. O'Dell, Tunable Alexandrite lasers, IEEE J. Quantum Electron., QE16, P.1302, (1980).

10) J.C. Walling, D.F. Heller, H. Samelson, D.J. Harter, J.A. Pete, and R.C. Moris, Tunable alexandrite lasers: Development and performance, IEEE J. Quantum Electron., QE-21, P.1568, (1985).

11) M.L. Shand and S.T. Lai, CW laser pumped emerald laser, IEEE J. Quantum E;ectron. QE-20 P.105, (1984).

12) B. Struve and G. Huber, Laser performance of Cr^{3+} : Gd(Sc,Ga) garnet, J. Appl. Phys., 57, p.45 (1985).

13) G. Huber and K. Petermann, Laser action in Cr-doped garnets and tungstates, in Tunable Solid State Lasers. P. Hamerling. A.B. Budgor, and A. Pinto. (Ed. Berlin: Springer Verlag) P.11-19 (1985).

14) J. Drude, B. Struve, and G. Huber, Tunable room temperature CW laser action in Cr^{3+}: GdScAl-garnet, Opt. Commun., 50, P.45 (1984).

15) J.A. Caird S.A. Payne, P.R. Straver, A.J. Ramponi, L.L. Chase, and W.F. Krupke, Quantum electronic properties of the $Na_3Ga_2Li_3F_{12}:Cr^{3+}$ laser.

16) U. Brauch and U. Dûrr. $KZnF_2$: Cr^{3+} A Tunable Solid state NIR laser Opt. Commun., 49, 61, (1984).

17) J.A. Craid, P.R. Staver, M.D. Shinn, H.J. Guggenheim, and D. Bahnck, Laser pumprd laser measurements of gain and loss in $SrAlF_5$: Cr crystals, in Tunable Solid state Lasers II, (eds. A.B. Budgor L. Esterowitz, and L.G.DeShazer) Springer Verlag , P.159-164 (1986).

18) H.P. Jensen and S.T. Lai, Tunable laser characteristics and spectroscopic properties of $SrAlF_5$:Cr., J. Opt. Soc Amer., B3, 115, (1986).

19) W. Kolbe, K. Petermann, and G. Huber, Broadband emission and laser action of Cr^{3+} doped zinc tungstanate at 1 μm wavelength. IEEE. J. Quantum Electron., QE21, 1596, (1985).

20) K. Petermann and P. Mitzscherlich, Spectroscopic and laser properties of Cr^{3+} doped $Al_2(WO_4)$, and $Sc_2(WO_4)$, IEEE J. Quantum Electron., QE-23, 1122 (1987).

21) S.T. Lai, B.H.T. Chai, M. Long, and R.C. Morris, $ScBO_3$: Cr^{3+} A room temperature near infrared tunable laser IEEE J. Quantum Electron., QE-22, 1931 (1986).

22) A.A. Kaminskii, A.P. Shkaderevich, B.V. Mill, V.G. Koptev, and A.A. Demidovich, Wide band tunable stimulated emission from a $La_3Ga_5SiO_{14}:Cr^{3+}$ crystal: Inorg. Mater., 23, 618, (1987).

23) L.J. Andrews, G.H. Beall, A. Lempecki, J. Lumin. 36, 65 (1986).

24) P.W. McMillan, in Glass-Ceramics (eds. J.P. Roberts and P. Popper), Academic Press, P.7 (1964).

25) Materials Advisory Board, Nat. Acad. Sci. Res. Council MAB P.243, (1968).

26) S.R. Elliott, Physics of Amorphous Materials, Longman Group Limited, New York, P.14 (1984).

27) Turnbull, D. Contemp. Phys., 10, 476, (1969).

28) G. Tamman, in The States of Aggregation, D. Van (Norstrand & Co., New York)

29) P.W. McMillan, in Glass-Ceramics (eds. J.P. Roberts and P. Popper), Academic Press P.27 (1964).

30) Doremus in Glass Science, Willey Interscience John Willey & Sons P 44 (1973).

31) G.H. Beall and D.A. Duke, in Glass: Science and Technology (eds. D.R. Uhlmann and N.J. Kreidl vol.1) 1983 Academic Press, New York.

32) R.D. Maurer, J. App. Phys., 33, 2132, (1962).

33) J.F. Mcdowell, G.H. Beall, J. Am. Cer. Soc., 52, 17, (1968).

34) Inorganic Electronic Spectroscopy, A.P. Lever Elsevier P.161 (1968).

35) L.E. Orgel, J. Chem. Soc., 4756, (1952).

36) S. Sugano, Y. Tanabe and H. Kamimura, in Multiplets of Transition Metal Ions in Crystals, Academic Press P.295, 296 (1970).

37) R.P. Bauman, Absorption Spectroscopy, John Wiley & Sons, Inc., New York, P.242, 248 (1962).

38) Z. Strand in:, Glass-Ceramic Materials, Glass Science and Technology vol.8 Elsevier P.171 (1986).

39) N.J. Kreidl in Glass Science and Technology (eds. D.R. Uhlmann and N.J. Kreidl) vol.1 P.107 Academic Press New York (1983).

40) A. Lempicki, L. Andrews, S.J. Nettel, B.C. McCollum, and E.I. Solomon, Phys. Rev. Lett. 44 1234 (1980).

41) L. Andrews, A. Lempicki, and B.C. McCollum, J. Chem. Phys. 74, 5526 (1981).

42) S.A. Payne, L.L. Chase, H.W. Herbert, L.K. Smith, and W.F. Krupe, J. Quantum. Electron. 24, 2243, (1988).

43) P. Kisliuk and C.A. Moore, Phys. Rev. 160, 307 (1967).

44) J.C. Walling , J. Quantum. Electron. QE-16, 1302 (1980).

45) L.J. Andrews, G.H. Beall, A. Lempecki, J. Lumin. 36, 65 (1986).

46) Photochemistry of Coordination Compounds, V. Balzani and V. Carassiti (Academic Press, New York) P. 64 (1970).

47) Inorganic Chemistry: Principles of Structure and Reactivity, J.E. Huheey, (Harper and Row) P.360 1978.

48) J. Zarzycki " Les verres et l'état vitreaux, Paris, Masson, 391.

49) C.R. Bamford, Phys. Chem. Glasses 3, 189 (1962).

50) T. Bates, in Modern Aspects of the Vitreous State, (ed. J.D. Makenzie (Butterworths, London, 1962), p.195.

51) R.E. Tischer, J. Chem. Phys. 48, 4291 (1968).

52) L.J. Andrews, A. Lempicki, and B.C. McCollum, J. Chem. Phys. 74

53) P.T. Kenyon, L. Andrews, B.C. McCollum, and A. Lempicki, J. Quantum Electron. QE-18, 1189 (1982).

54) A.M. Glass, J. Chem. Phys. 50, 1501, (1969).

55) G. Boulon, B. Moine, J.C. Bourcet, R. Reisfeld, and Y. Kalisky, J. Lumin. 18,19, 924, (1979).

56) T.H. Keil, Phys. Rev., 140 2A , A601, (1965).

57) M. Bouderbala, G. Boulon, R. Reisfeld, A. Buch, M.I. Shalom, A.M. Lejus, Chem. Phys. Lett., 121, 535, (1985).

58) A.J. Wojtowicz, W. Meng, A. Lempicki, G.H. Beall, D.W. Hall, and T.C. Chin, J. Quantum. Electron., 24, 1109, (1988).

59) R. Reisfeld. A. Kisilev, A. Buch, M. Ish-Shalom, J. Non-Cryst. Solids, 91, 333 (1987).

60) R. Reisfeld, A. Kisilev, and E. Greenberg, Chem. Phys. Lett. 104 153 (1984).

61) E.M. Levin, H.F. McMurdie and F.P. Hall, Phase Diagram For Csramitists, The American Ceramic Society (1956).

62) A.L. Schawlow, D.L. Wood and A.M. Clogston, Phys. Rev. Lett. 3, 271 (1959).

63) R.C. Powell, B. di Bartolo, B. Birang, and C.S. Naiman, Phys. Rev. 155 296 (1967).

64) G.F. Imbush and R. Kopelman, in Topics in Applied Physics (eds. W.M. Yen and P.M. Selzer) Vol. 49, Springer-Verlag , Berlin Heidleberg New York (1981)

65) M.J. Henry, J.P. Larkin, G.F. Imbush, Phys. Rev. B, 13, 1 (1976).76).

66) F. Durville, B.Champagnon, E. Duval, G. Boulon. F. Gaume A,F. Wright, A.N. Fitch, Phys. and Chem. of Glasses., 25, 126 (1984).

67) J. Derkosch, W. Mikenda, and A. Preisinger, Spectrochim. Acta. 32A, 1759 (1981).

68) W. Mikenda, A. Preisinger, J. Lumin., 26, 67 (1981).

69) W. Mikenda, J. Lumin., 26, 53 (1981).

70) F. Durville, B. Champagnon, E. Duval and G. Boulon J. Phys. Chem. Solids, 46, 701, (1985).

71) V.K. Malinovsky, V.N. Novikov and A.P. Sokolov, Sol. State Comm., 57 725, (1988)

72) A.J. Wojtowicv and A. Lempicki, J. Lumin. 39, 189 (1988).